RICE UNIVERSITY

# A structure-function characterization of the ER membrane protein atlastin

by

**Tyler J Moss**

A THESIS SUBMITTED
IN PARTIAL FULFILLMENT OF THE
REQUIREMENTS FOR THE DEGREE

**Doctor of Philosophy**

APPROVED, THESIS COMMITTEE

Dr. James A. McNew, Associate Professor of Biochemistry & Cell Biology

Dr. Yizhi Jane Tao, Associate Professor of Biochemistry & Cell Biology

Dr. Charles R. Stewart, Professor of Biochemistry & Cell Biology

Dr. Huey W. Huang, Sam and Helen Worden Professor of Physics and Astronomy

HOUSTON, TEXAS
OCTOBER 2011

# Abstract

## A structure-function characterization of the ER membrane protein atlastin

by

**Tyler Moss**

The biogenesis and maintenance of the entire endomembrane system is dependent upon membrane fusion proteins. Mounting evidence indicates that the integral membrane GTPase Atlastin is a membrane fusion protein involved in the homotypic fusion of the endoplasmic reticulum (ER) membrane suggesting a role in the biogenesis and maintenance of ER structure. I helped show that recombinant *Drosophila* atlastin is able to promote the fusion of synthetic membranes in vitro and that this fusion is dependent upon atlastin GTPase activity. The structure-function experiments presented here assist in elucidating domains required in the mechanism of atlastin mediated membrane fusion. ER homotypic fusion is dependent upon the self-association of Atlastin subunits in adjacent membranes to bring the bilayers into close molecular contact. Atlastin dimerization occurs in the presence of GTPγS but not GDP and stable dimerization is dependent upon a juxtamembrane middle domain three-helix bundle (3HB). The atlastin GTPase domain and 3HB form a potent soluble domain inhibitor of atlastin homotypic fusion, while the GTPase domain alone shows little inhibition. Designed GTPase domain mutations show that GTP binding and atlastin dimerization is insufficient to

support fusion without GTP hydrolysis. Additionally, domain analysis of atlastin reveals that the C-terminal cytoplasmic domain of atlastin is absolutely required for membrane fusion, possibly through a protein-lipid interaction of an amphipathic alpha-helix. Genetic lesions in the human Atlastin-1 gene, SPG3A, result in a form of autosomal dominant hereditary spastic paraplegia (HSP). A better understanding of Atlastin function should lend significant insight into normal ER biogenesis and maintenance, as well as the pathology of human disease.

# Acknowledgments

Firstly, I want to acknowledge Dr. James McNew for his mentorship. Thank you for accepting me into you lab and teaching me everything that I have learned over these past 5 years. Thank you for fostering the perfect environment where I always felt that I could try new things. This helped me to break free from the written protocols and instruction manuals and attack problems from new angles yet feel comfortable that there was a wealth of expertise to buoy me up when I started to tread water. Thank you for understanding that I had a life outside of school. I always felt like I was a person first and not just a pair lab hands. Thanks for being a friend.

I want to thank past committee members, Dr. Richard Gomer, Dr. Michael Gustin, and Dr. Ronald Perry and current committee members; Dr. Jane Tao, Dr. Charles Stewart , and Dr. Huey Huang. Thank you for your questions and suggestions. Thank you for your time.

I thank all the members of the McNew lab, Dr. Blaire Doneske, Dr. Travis Rodkey, Joseph Faust, Avani Verma, and Tanvi Desai, for their help and friendship. I especially want to thank Dr. Song Liu for all the good times I had as a new lab member working late into the night and having fun while we were at it. Thank you for your patience in helping me with all my experiments and for getting me started on this Atlastin project. And mostly, thank you for your friendship.

Most of all I want to thank my wife for her love and support. You were always understanding and patient with a husband who had to work late some nights and work hard through some weekends. Thank you for your encouragement and belief in me.

# Contents

# List of Figures

# List of Tables

# List of Equations

# List of Definitions

| | |
|---|---|
| 2DSA | two-dimensional spectral analysis |
| $^{3}H$ | tritium |
| 3HB | 3-helix bundle |
| ABD | 7-amino-2,1,3-benzoxadiazol |
| ADHSP | autosomal dominant hereditary spastic paraplegia |
| Amp | ampicillin |
| ARHSP | autosomal recessive hereditary spastic paraplegia |
| Atl | atlastin |
| ATL1 | atlastin-1 |
| AUC | analytical ultracentrifugation |
| bp | base pair |
| CLIMP-63 | cytoskeleton-linking membrane protein (63 kDa) |
| CNS | central nervous system |
| Da | Dalton |

| | |
|---|---|
| DLS | dynamic light scattering |
| DNA | deoxyribonucleic acid |
| DOPS | dioleoylphosphatidylcholine |
| DPPE | dipalmitoylphosphatidylethanolamine |
| DTH | dithionite |
| EDTA | Ethylenediaminetetraacetic acid |
| EM | electron microscopy |
| ER | endoplasmic reticulum |
| FLIP | fluorescence loss in photobleaching |
| $F_{max}$ | maximum fluorescence |
| $F_{min}$ | minimum fluorescence |
| FRET | fluorescence resonance energy transfer |
| GDP | guanosine diphosphate |
| GFP | green fluorescent protein |
| GMP | guanosine monophosphate |
| GMPPNP | 5'-Guanylyl imidodiphosphate |

| | |
|---|---|
| GSH | glutathione |
| GST | glutathione S-transferase |
| GTP | guanosine triphosphate |
| GTPγS | guanosine 5'-O-[gamma-thio]triphosphate |
| HA | Hemagglutinin |
| HEK293 | Human Embryonic Kidney 293 cells |
| HEPES | 4-(2-hydroxyethyl)-1-piperazineethanesulfonic acid |
| hGBP1 | human guanylate-binding protein 1 |
| HPLC | high-performance liquid chromatography |
| HSP | Hereditary Spastic paraplegia |
| IPTG | isopropyl-β-D-1-thiogalactopyranoside |
| $K_d$ | equilibrium dissociation constants |
| kDa | kiloDaltons |
| $K_m$ | Michaelis constant |
| LB | lysogeny broth |
| $LN_2$ | liquid nitrogen |

| | |
|---|---|
| LUV | large unilamellare vesicles |
| mant | N-methylanthraniloyl |
| MESG | 2-amino-6-mercapto-7-methylpurine riboside |
| $N_2$ | nitrogen |
| NBD | 7-nitro-2-1,3-benzoxadiazol-4-yl |
| OD | optical density |
| PCR | polymerase chain reaction |
| PDI | Protein disulfide isomerase |
| PNP | purine nucleoside phosphorylase |
| POPC | 1-Palmitoyl-2-oleoylphosphatidylcholine |
| REEP1 | receptor expression enhancing protein 1 |
| Rh | rhodamine |
| RHD3 | root hair defective 3 |
| RNAi | RNA interference |
| SAXS | small-angle x-ray scattering |
| SDS-PAGE | sodium dodecyl sulfate polyacrylamide gel electrophoresis |

| | |
|---|---|
| SENP2 | Sentrin-specific protease 2 |
| Sey1p | synthetic enhancer of yop1 |
| SNARE | SNAP (Soluble NSF Attachment Protein) REceptor |
| SPAST | Spastin |
| SPG | SPastic Gait |
| SUMO-1 | Small Ubiquitin-like Modifier |
| TBAB | tetra-n-butylammonium bromide |
| TCEP | Tris(2-carboxyethyl)phosphine |
| TEM | transmission electron microscopy |
| TMD | transmembrane domain |
| Tris | 2-Amino-2-hydroxymethyl-propane-1,3-diol |
| UAS | upstream activation sequence |
| $V_{max}$ | maximum velocity |
| WT | wildtype |
| βME | β-mercaptoethanol |

Chapter 1

# Introduction and Literature Review

Biological membranes are one of the defining characteristics of living organisms and are essential to life. Biological membranes are composed of amphipathic lipids that form lipid bilayers spontaneously to protect the hydrophobic tails from aqueous solution and expose the polar heads groups to the surrounding aqueous environment. Lipid bilayers assume an energetically favorable spherical structure forming a semipermeable membrane which defines the limits of a cell. Eukaryotic organisms also have intracellular membranous compartments. The formation and maintenance of these compartments and transfer of compartmental material from one compartment to the next requires membrane fusion. The fusion of biological membranes is an essential process in all eukaryotic cells. All known biological membrane fusion is mediated by specific fusion proteins or fusogens.

## 1.1. Biological membrane fusion

Membrane fusion is defined as the merging of two separate lipid bilayers followed by the mixing of their bound aqueous contents. In biological systems membrane fusion is not a spontaneous process. There are several energy barriers that must be overcome prior to lipid and aqueous content mixing. A significant amount of energy input is required in order to displace the water shell surrounding the two lipid bilayers, overcome the barriers of electrostatic repulsion between the phospholipid polar head groups, and then disrupt two continuous lipid monolayers[1](Figure 1-1). The high curvature of vesicle membranes can overcome some of these energy barriers, but it is apparent that membrane fusion requires more than just close membrane apposition[2]. The remaining energy needed is provided by fusion peptides, which are vital to many cellular processes that require the fusion of biological membranes[3]. It has been proposed that all intracellular fusion events are mediated by fusion proteins [4]. The fusion of biological membranes can be divided into three broad categories: viral fusion, cell-cell fusion, and intracellular fusion (Figure 1-2). Viral fusion (the fusion of a viral membrane with

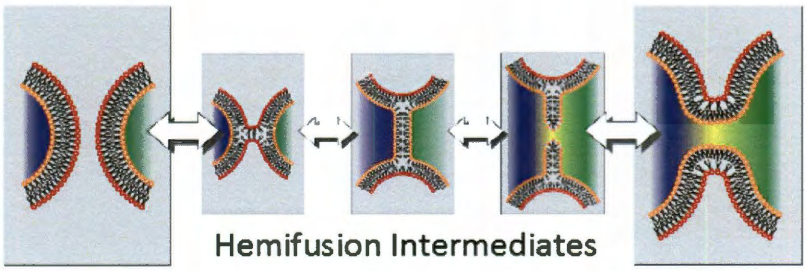


**Figure 1-1: Membrane fusion proceeds through hemifusion**
Membrane fusion begins when two membranes are brought into close proximity, followed by the mixing of outer-leaflets and fusion stalk formation, expansion of the stalk to form a fusion diaphragm, and mixing of inner-leaflets to form fusion pore and mixing of aqueous contents.

the host cell membrane) is a necessary part of viral pathogenesis. Cell-cell fusion is important in many developmental processes and is necessary for fertilization. The last type of fusion, intracellular fusion, is important in many processes that occur inside the eukaryotic cell.

Intracellular fusion included all the fusion events in the secretory and endocytic pathways. Other types of intracellular membrane fusion include organelle

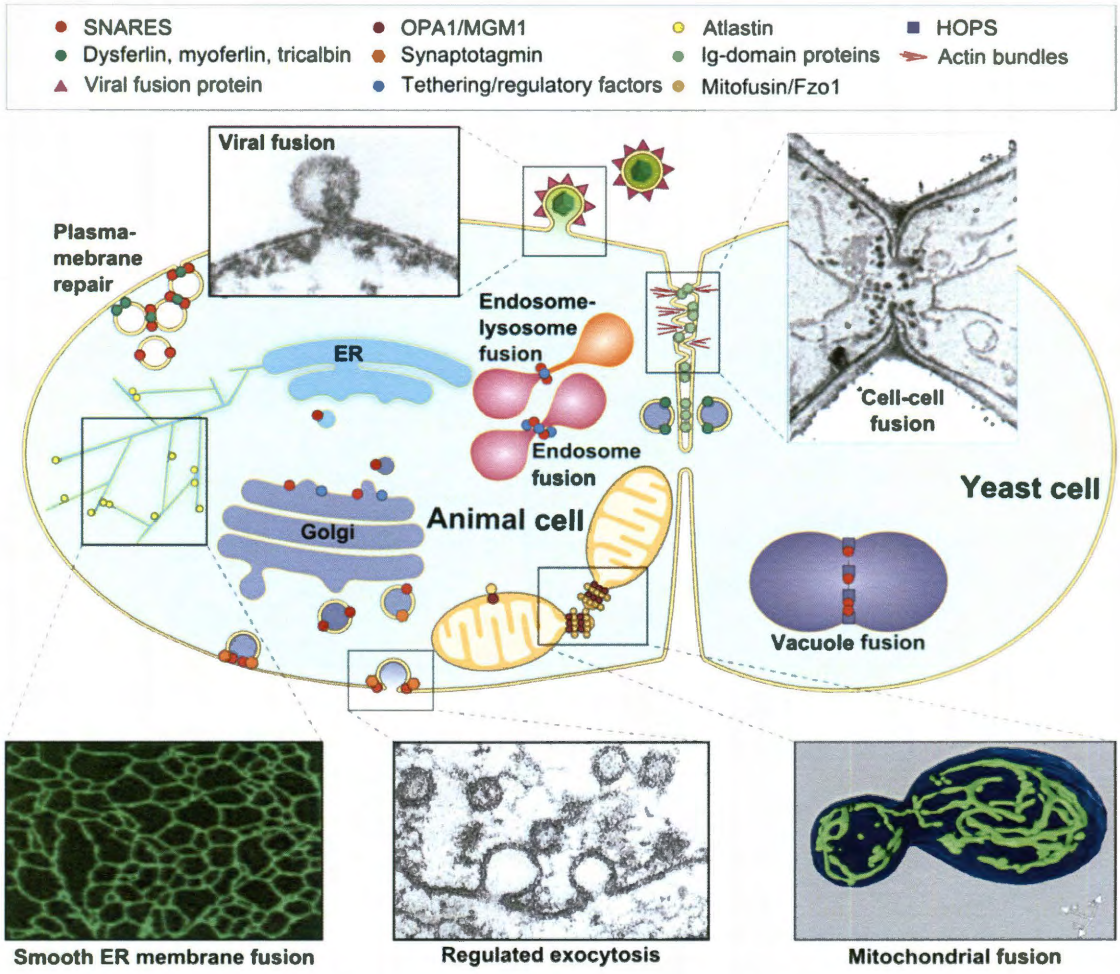


**Figure 1-2: The fusion of biomembranes is essential to many cellular functions.** A diagram of two generic cells depicts several cellular processes that require membrane fusion and the proteins that mediate the fusion. Electron micrographs show viral-cell (top-left) and cell-cell fusion (top-right). Fusion is essential for peripheral ER (bottom left) formation, exocytosis (bottom middle) and mitochondrial network formation and maintenance (bottom right). Adapted from Martens and McMahon (2008)

fusion. The biogenesis and maintenance of several organellar structures, such as peroxisomes, the endoplasmic reticulum, mitochondria, and vacuoles, requires both fusion and fission.

## 1.2. Endoplasmic reticulum membrane fusion

The endoplasmic reticulum (ER) is also a highly dynamic organelle that exists as an interconnected network of tubes and sheets[5-7]. While ER sheets are mostly perinuclear and contiguous with the outer nuclear envelope, peripheral tubular extensions of the ER move along microtubule tracks frequently joining together by membrane fusion. Regions of the peripheral ER maintain close contact with virtually all other cytoplasmic organelles including mitochondria, peroxisomes, chloroplasts, Golgi and the plasma membrane. These diverse associations throughout the cytoplasm may be one reason the ER is structured as a diffuse network in the cell periphery. These extensive connections likely play a functional role in non-vesicular transport of ER-synthesized lipids and sterols as well as inter-organelle calcium homeostasis. Membrane fusion allows the ER to maintain a dynamic network that can quickly change shape and preserve lumen continuity while adapting to the changing cytoplasmic environment.

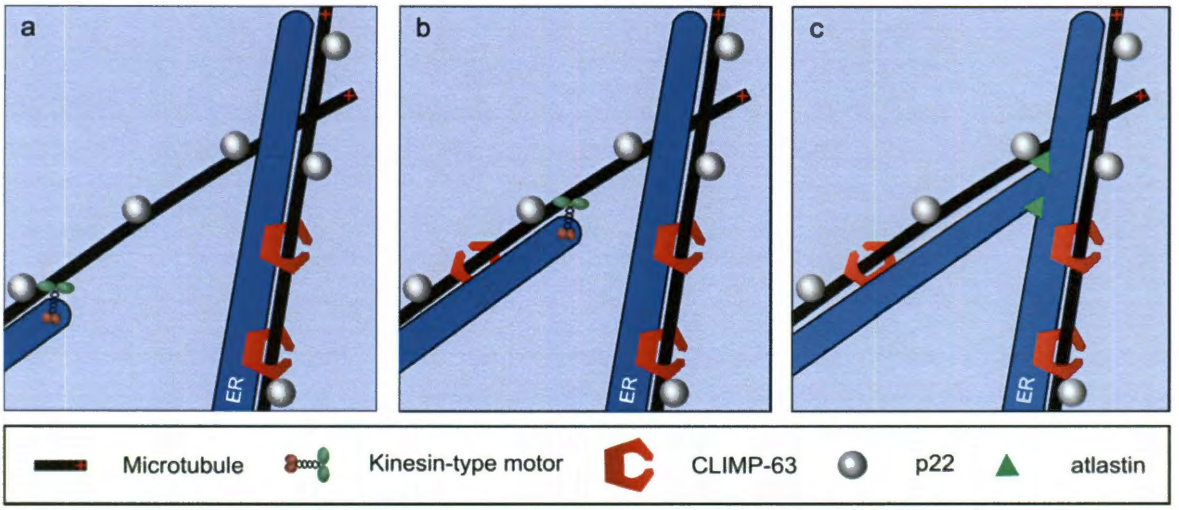


**Figure 1-3: The formation of three-way junctions in the reticular ER by membrane fusion.** The reticular morphology of the peripheral ER is formed by the expansion of ER tubules along microtubule tracks pulled by kinesin motors (**a-b**). ER tubule ends come into contact with adjacent tubules and protein-mediated fusion occurs to form three-way junctions (**c**) leading to the overall network structure of the peripheral ER. Adapted from Vedrenne (2006).

The tubular ER forms a dynamic network of interconnected tubules that are continuously rearranged through fission and fusion of the ER membrane[8]. Fusion and fission are required to maintain the complex morphology of the ER. As membrane tubules extend into the cytoplasm along microtubules, they fuse with other tubules to form the reticular morphology of the tubular ER[9]. BNIP, the p97 protein complex, and SNARE proteins have been suggested as being responsible for the homotypic fusion of ER membranes[10,11], however, none of these proteins exhibit the GTPase activity which is necessary for this process[12]. We, along with others, have shown that the ER localized large GTPase atlastin is directly responsible for the fusion of ER membranes[13,14].

## 1.3. Atlastin

### 1.3.1. SPG3A and HSP

Atlastin is encoded by the human SPG3A (SPastic Gait or SPastic parapleGia 3A) locus[15]. Mutation of SPG3A is responsible for a form of Hereditary Spastic Paraplegia (HSP, also called familial spastic paraparesis or Strümpell-Lorrain disease), a group of inherited neurological disorders characterized by progressive lower extremity weakness and spasticity[16,17]. Clinical presentation varies significantly with age from very young children to adults as old as 55 years. The neuropathological basis for compromised motor function in HSP is likely length dependent axonopathy of the corticospinal tract[17]. Genetic analysis has identified 38 different loci involved in HSP (*SPG1-45*)[16–18]. All methods of inheritance have been reported including autosomal dominant (ADHSP), autosomal recessive (ARHSP) and X-linked HSP. ADHSP is by far the most prevalent[19]. Seventeen HSP loci have been identified and their molecular analysis has yielded three main categories of potential causation. These gene functions fall into three broad groups including intracellular trafficking, mitochondrial function, and axonal pathfinding and myelination[20]. Over half of all ADHSP cases occur in one of three proteins: Spastin (*SPAST*, *SPG4*,), Atlastin-1 (*ATL1*, *SPG3A*), and receptor expression enhancing protein -1 (*REEP1, SPG31*). Spastin mutations occur in 40-45% of ADHSP[21], while Atlastin-1 and REEP1 account for 10%[22] and 3% respectively.

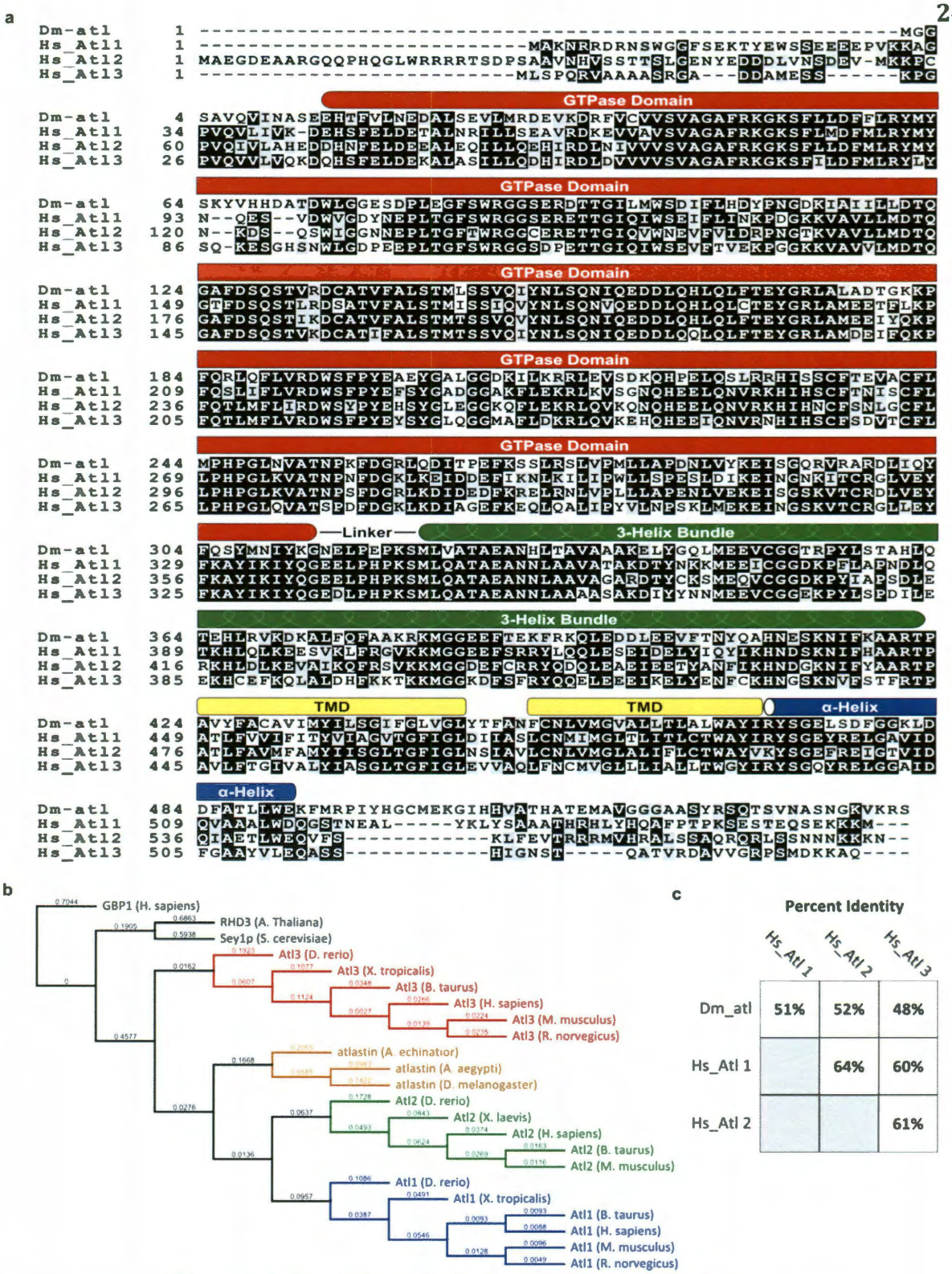


**Figure 1-4 Comparison of atlastin orthologs and paralogs.**

(**a**)An annotated multiple sequence alignment (ClustalW) of atlastin (black shading = identical residues, gray shading = similar residues). (**b**) Cladogram of atlastin orthologs and paralogs with hGBP1 as an outgroup (blue, atlastin-1 isoforms; green, atlastin-2 isoforms; red, atlastin-3 isoforms; brown, organisms with single isoforms). (**c**) Comparison of percent identity between fly atlastin and human atlastin isoforms.

Molecular analysis of patients with HSP has identified 34 point mutations, 3 frame shifts and one single amino acid deletion in the *ATL1* gene (Table 5- 1). All of these lesions are dominant alleles and mutations have been identified in all domains of the protein. Dominant inheritance suggests that the mutant protein is an either dominant loss of function allele due to haploinsufficiency, a gain of function allele, or a dominant negative allele. The fact that all of the 38 mutations yield a common phenotype strongly argues against a gain of function allele. The most likely pathological mechanism is therefore haploinsufficiency or a dominant negative protein.

Human atlastin-1 (Atl1) is a 558 amino acid (63,544 Da) multidomain protein (Figure 1-4). It has a short N-terminal domain, followed by a well-conserved GTPase domain, a middle domain with that forms a 3-helix bundle (3HB), two tandem transmembrane domains and a C-terminal cytoplasmic domain[23]. The original atlastin gene was renamed atlastin-1 following the identification of two additional paralogs (atlastin-2 and atlastin-3)[23].

### 1.3.2. Atlastin subcellular localization

Several groups have analyzed the relative abundance and subcellular distribution of the human atlastins. Antibodies against Atl1 recognize a protein of the appropriate size predominantly in human brain, but smaller amounts also in other tissues[23]. Immunocytochemsitry in rat brain sections found strong staining in pyramidal cells in layer V of the cerebral cortex and pyramidal neurons in the hippocampus. Atl1 colocalized with the Golgi marker p115, but not with anti-KDEL

antibodies that mark the ER suggesting that the Atl1 was a Golgi resident protein. Golgi localization in cultured rat neurons was also suggested by electron microscopy and immunogold labeling. Subsequent localization studies[24] found that myc-tagged-Atl1 and Atl1-GFP both strongly co-localized with calreticulin, PDI, and sec61alpha in HeLa and NSC34 cells providing evidence for an ER localization. The Golgi marker GM130 displayed a distinctly different distribution than Atl1-GFP10. Yet a third group localized transfected Atl1 mainly to the ER in HEK293 cells[25]. Localization studies of Atl2 and Atl3 found that these paralogs were both localized to the ER[26], further supporting the growing consensus that atlastins are ER resident proteins.

### 1.3.3. Atlastin interacting proteins

Atl1 has been shown to associate with Spastin, a microtubule severing protein, in some contexts[5,6,24], and recent work has also demonstrated that atlastin interacts with all of the ER tubule forming proteins in the Reticulon and REEP/Yop/DP1 family[6,14]. An interaction between Atl1 and spastin has been reported by several groups[5,6,24,26], but often with contradictory conclusions. An unspecified partial coding sequence of Atl1 was identified in a yeast-two hybrid screen with spastin as bait[24]. GST-pull down experiments suggested that GST full-length Spastin was able to weakly bind the Myc-tagged N-terminal cytoplasmic domain of Atl1 (myc-Atl1ΔTMD) from cell extracts. Additional two hybrid interaction data and GST pull downs found that the N-terminal 80 amino acids of spastin were necessary for the spastin-myc-Atl1ΔTMD interaction. Spastin-Atl1 interactions were also probed by coimmunoprecipitation experiments[24]. Myc-

spastin and Atl1-GFP were co-overexpressed in HEK293T cells and Atl1-GFP precipitated with anti GFP antibodies. A very small amount of myc-spastin was detected in the precipitates. Surprisingly, however, no association was detected when antibodies to native proteins were used for immunoprecipitation. Apparently, spastin interaction with atlastin is limited to atlastin-1, since atlastin-2 and atlastin-3 do not interact with spastin[26].

A second two-hybrid study also identified Atl1 when spastin was used as bait to screen a library [5]. Surprisingly, this work found that the C-terminus (residues 408-558) of Atl1 interacted with full length human Spastin. In vitro experiments suggested that the GST-Atl1 tail (495-558) retains some cleaved (GST)-Spastin. An interaction between full-length HA-tagged spastin and His6-tagged Atl1 was also detected by coimmunoprecipitation from HeLa cells.

Most recently, an association between three HSP proteins atlastin, spastin and REEP1 has been reported[6]. This work showed that the interaction between atlastin and REEP1 likely occurs through hydrophobic membrane spanning domains of each protein[6], similar to the other tubule forming proteins[14]. A similar observation was made for the interaction of spastin with atlastin suggesting that region of interaction between these two proteins is the N-terminal transmembrane segment of the M1 isoform[6] of spastin and the two tandem TMDs of atlastin.

In summary, a substantial but contradicting amount of data suggest that Atl1 and spastin interact, but the nature and significance of this interaction remains obscure.

### 1.3.4. Previous work on atlastin

Atlastin function has been examined also in model organisms, specifically the fruit fly Drosophila melanogaster. The Drosophila genome produces a single atlastin protein. Drosophila Atlastin is 541 amino acids long and has a predicted molecular weight of 60,927 Da (Figure 1). The drosophila atl sequence is highly homologous with all three human isoforms ranging between 48-51% identical (61-68% similar) over the entire length of the protein. Functional homologs of atlastin are also found in yeast (Sey1p) and plants (RHD3) as well[14,27]. These proteins share limited sequence similarity with human atlastin, yet these GTPases possess a similar domain structure and potential function.

The first phenotypic characterization of atlastin function in Drosophila was reported in 2008. Lee et al. identified a P-element insertion in the fly atlastin gene (atl1) during a large scale behavioral screen[7]. These authors noted that this mutant was temporarily paralyzed by mechanical shock and classified it as "bang-sensitive". Molecular analysis of this P-element insertion indicated that neither transcript from the drosophila atlastin gene was made and no protein was produced when fly extracts were examined by immunoblotting. This mutant was viable, but sterile due to problems with oocyte development. atl1/ atl1 homozygous flies are much smaller than their wildtype counterparts and have a reduced lifespan, ~55% shorter than control animals. Behavior abnormalities were examined in undisturbed flies and animals that had been exposed to mechanical stress. The stressed animal exhibited mobility defects that worsened with age leading the authors to speculate

that problems with dopaminergic neurons may be occurring. Examination of wildtype and atl1 brains found that the number dopamineric neurons were reduced and the reduction was more pronounced with increasing age. Reintroduction of atlastin on a genomic transgene fragment prevented the loss of these neurons. Additionally, selective reexpression in dopamineric neurons using a UAS transgene also improved the loss of mobility of atl1 mutants.

Given the potential importance of the observed age related loss of dopamineric neurons in Drosophila to the pathophysiology of HSP, Albin et al.[28] examined dopaminergic nigrostriatal innervation in SPG3A ADHSP patients, but found normal nigrostraital terminal densities in both affected individuals suggesting that degeneration of dopamineric neurons is not a common course in humans. This observation is also consistent with the clinical presentation of SPG3A ADHSP at an early age and slow or no progression.

More recently, another atlastin mutant (atl2) was generated by imprecise excision of the original atl1 P-element[29]. No rationale was provided for the generation of this new mutant given that their previous report documented that the atl1 P-element insertion was a null allele. Regardless, the new ~1,600 bp deletion mutant is likely a null alelle and is pupal lethal with ~8% adult escaper that are sterile. This result strongly suggests that the original P-element insertion (atl1) was not a null allele and casts doubt on the original observations made with this fly line.

Immunolocalization experiments found that drosophila atlastin was broadly expressed in the larval CNS as well as body wall muscle, but not enriched within

synapses. Subcellular localization in muscle found that the majority of fly atlastin was localized to the ER, marked by GFP-KDEL.

Analysis of the atl2 mutant indicated that loss of Atlastin produced subtle effects on synaptic bouton number as well as body wall muscle size in wandering third instar larvae. Examination of microtubule organization in muscle suggested that atlastin may regulate microtubule organization and dynamics, as has been suggested by association with spastin. Furthermore, these authors suggest that atlastin may also functionally and physically interact with Spastin. Overexpression of atlastin in muscle yielded a decrease in the amount of acetylated tubulin detected by immunofluorescence and loss of spastin reversed this effect. Finally, in vitro GST pull down experiments indicated that a very small amount of myc-tagged atlastin in HEK293 cell extracts can be isolated with the N-terminus of Spastin fused to GST.

# Chapter 2

# Materials and Methods

## 2.1. Molecular biology

### 2.1.1. Expression vectors

Prior to expression of recombinant protein I subcloned atlastin and atlastin mutants into a modified pGEX-4T-3 vector. To make the modified vector complementary, 5′-phosphorylated oligonucleotides ( #594 (5′-TCG AGC ATC ATC ATC ATC ATC ATC ACT GAC-3′) and #595 (5′-GGC CGT CAG TGA TGA TGA TGA TGA TGA TGA TGC-3′)) were mixed together and ligated into pGEX-4T-3 cut with XhoI and NotI to generate **pJM680** (pGEX-4T-3 with a carboxy-terminal octa-histidine tag).

An additional expression vector, **pGEX-ST**, was used for the production of untagged proteins. pGEX-ST is a bacterial expression vector that contains an N-terminal GST-SUMO tag[30]. The first 97 residues of SUMO-1 is inserted after the GST

sequence and upstream of the BamHI cut site so that when the expressed protein is cut with SENP2 it results in a protein with its native methionine as the N-terminal residue. This vector and a plasmid containing the sequence encoding *Drosophila melanogaster* atlastin (1-328) in pGEX-ST (**pJM841**) was graciously donated by our collaborator (Mariko Aryoshi; Kyoto University, Japan).

### 2.1.2. Subcloning

*Drosophila melanogaster* atlastin was PCR amplified from pGEX-atlastin (obtained from Andrea Daga) using the oligonucleotides #583 (5′-CCG GAT CCA TGG GCG GAT CGG C-3′) and #590 (5′-ATC TCG AGT GAC CGC TTC ACC-3′), digested with BamHI and XhoI, and ligated into pJM680 cut with the same enzymes to generate **pJM681**.

The c-terminal truncations of atlastin were generated by PCR using pJM681 as a template. The sequences corresponding to atlastin (1-422), **pJM704**; atlastin (1-450), **pJM705**, atlastin(1-471), **pJM706**, and atlastin(1-497), **pJM813** were amplified using the forward oligo #583 and the reverse oligos #611 (5′-ATC TCG AGT GTC CGT GCT GCC-3′), #612 (5′-TTC TCG AGG TTG GCG AAC GTA TAG AGA CC-3′), #613 (5′-CCC TCG AGA TAT CTA ATG TAG GCC CAC-3′), and #687 (5′-ATC TCG AGG ATG GGT CGC ATG AAT TTC TC-3′), respectively. The PCR product was cut with the restriction enzymes BamHI and XhoI and ligated into pJM680 cut with the same enzymes. All of the clones were confirmed by DNA sequencing.

Point mutations within the GTPase domain and 3HB were generated by members of Andrea Daga's lab. To make the GST-tagged GTPase domain point mutants, atlastin$^{K51A}$ (**pJM694**), atlastin$^{R214C}$ (**pJM727**), atlastin$^{S234Y}$ (**pJM728**), and atlastin$^{R48A}$ (**pJM815**), the mutant DNA sequences were digested using the unique restriction sites PpuMI and SphI within the Drosophila atlastin sequence. The restriction fragments were ligated into pJM681 cut with the same enzymes. Soluble domain mutants were made by using the same enzymes and ligating the K51A and R48A point mutations into pJM704 to create **pJM746** and **pJM835**, respectively.

Similarly, the 3HB point mutations atlastin$^{L400A}$ (**pJM702**), atlastin$^{F404P}$ (**pJM703**), and atlastin$^{1xlinker}$ (**pJM724**), were digested with the unique restriction enzymes PpuMI and SacI and ligated into pJM681 cut with the same enzymes.

Atlastin(1-422) was moved to pGEX-ST by cutting pJM704 with the restriction enzymes BamHI and EagI and ligating the DNA fragment into pGEX-ST cut with the same enzymes to create **pJM781**. Cutting with EagI carried the C-terminal octa-histidine tag with the sequence.

### 2.1.3. Mutagenesis

Two point mutations within the c-terminal cytoplasmic domain, atlastinF478K (**pJM863**) and atlastinL482K (**pJM882**), were generated by overlap extension PCR[31]. The outside oligos #583 and #590 were used for both. The phenylalanine-478 to lysine mutation was introduced using the overlapping oligos #767 (5′-GGA GAG CTC AGC GAC AAA GGC GGC AAG TTG GAT G-3′) and #768 (5′-

CAT CCA ACT TGC CGC CTT TGT CGC TGA GCT CTC C-3′). The leucine-482 to lysine mutation was introduce using the overlapping oligos #790 (5′-CGA CTT TGG CGG CAA GAA GGA TGA CTT TGC AAC-3′) and #791 (5′-GTT GCA AAG TCA TCC TTC TTG CCG CCA AAG TCG-3′). The PCR products were cut with SphI and XhoI and ligated into pJM681 cut with the same enzymes.

Overlap extension PCR was also used to introduce a unique BspEI restriction site at residues serine-472 and glycine -473 of atlastin (**pJM865**) which are at the start of the c-terminal cytoplasmic domain. To do this the silent mutations 1413A>T and 1414G>C were made using the overlapping oligos #765 (5′-GCC TAC ATT AGA TAT TCC GGA GAG CTC AGC G-3′) and #766 (5′-CGC TGA GCT CTC CGG AAT ATC TAA TGT AGG C-3′) and the flanking oligos #583 and #590. The PCR product was cut with SphI and XhoI and ligated into pJM681 cut with the same enzymes.

The c-terminal cytoplasmic domain of drosophila atlastin (residues 473 to 541) was swapped with the c-terminal cytoplasmic domain of human atlastin-1 (**pJM866**, residues 499 to 558) and atlastin-3 (**pJM868**, residues 526 to 579). The corresponding DNA sequence from atlastin-1 was amplified using the oligos #771 (5′-ATT CCG GAG AAT ACC GAG AGC TGG-3′) and #777 (5′-ATC TCG AGC ATT TTT TTC TTT TCT GAT TGT TCA G-3′). The atlastin-2 DNA sequence was amplified with the oligos #773 (5′-ATT CCG GAC AAT ATC GTG AGC TGG GC-3′) and #635 (5′- TTC TCG AGT TGA GCT TTT TTA TCC ATG G -3′). The PCR products were cut with BspEI and XhoI and ligated into pJM865 cut with the same enzymes.

## 2.2. Protein expression and purification

A biochemical characterization of atlastin requires the isolation of purified protein. All recombinant protein was expressed in and purified from *Echerichia coli* BL21 (DE3) cells (Stratagene). The expression vectors used confer ampicillin (Amp) resistance to the cells. Cells were culture in lysogeny broth (LB)[32] and on LB-agar plates that contained 100 μg per ml Amp.

### 2.2.1. GST-tagged protein purification

GST-tagged proteins were produced starting by transforming *E. coli* BL21(DE3) (Stratagene) cells with the respective expression plasmid. Overnight colonies were picked to start pre-precultures in 5 ml LB + Amp. The pre-precultures were used to start 50 ml precultures that were grown overnight at 25°C. The cells from the 50 ml precultures were pelleted at 3,000 rpm (~2,000xg) for 15 min using an Allegra tabletop centrifuge at room temperature. The cell pellet was used to seed 2 to 4 L cultures with a starting density of about 0.1 to 0.2 optical density at 600 nm (OD). The cultures were grown at 25°C up to a desirable density (OD = 0.4 to 0.5) at which time the culture was moved to a 16°C incubator. Ten minutes after growth at 16°C, the protein expression was induced with 0.2 mM isopropyl-β-D-1-thiogalactopyranoside (IPTG) and the cultures were grown overnight (~16 hours) at 16°C. The cells were harvested, washed with 25 mM HEPES (pH 7.4) and 200 mM KCl and lysed in breaking buffer (25 mM HEPES (pH 7.4), 200 mM KCl, 10% glycerol, 2 mM 2-mercaptoethanol (βME), 4% Triton X-100, 2mM EDTA and 1X complete protease inhibitor cocktail (Roche)) by passage

through an Emulsiflex C-3 high pressure homogenizer (Avestin) twice at 15,000-20,000 psi. Cell extracts were cleared by centrifugation at 125,000 x (~186,000xg) for 30 min using a Type 45-Ti rotor in an Optima LE-80K ultracentrifuge (Beckman) cooled to 4°C. Cleared extracts were incubated with 70 mg of swelled glutathione (GSH)-agarose beads (Sigma) for 1 hr at 4°C.

GST-tagged proteins that have at least one transmembrane domain (pJM681, -694, -702, -703, -705, -706, -724, -727, -728, -813, -815, -863, -866, -868, and -882) were purified as follows. The GSH bead-bound protein was washed with 25 mM HEPES (pH 7.4), 100 mM KCl, 10% glycerol, 2 mM βME, 1% Triton X-100, and 1 mM EDTA . The protein was washed 5 more times with 10 ml of 25 mM HEPES (pH 7.4), 100 mM KCl, 10% glycerol, 2mM βME, 0.1% anapoe X-100, and 1mM EDTA. The protein was eluted from GSH-agarose with 25 mM HEPES (pH 7.4), 100 mM KCl, 10% glycerol, 2 mM βME, 0.1% anapoe X-100, 1 mM EDTA, and 10 mM GSH. Identical conditions were used for the soluble fragments of atlastin (pJM704, -746, and -835) with the exception that detergent was left out of the wash and elution buffers.

The proteins were analyzed by SDS-PAGE and coomassie stain and the protein concentration was determined by amido black protein assay[33]. Frozen aliquots were stored at -80°C.

### 2.2.2. GST-SUMO-tagged protein purification

For GST-SUMO-tagged proteins (pJM781 and pJM841) the cell growth and protein expression was the same as for the GST-tagged proteins. The washed cells were lysed in 20 mM Tris pH 7.5, 200 mM KCl, 10% glycerol, 2 mM βME, 2 mM EDTA, 1X complete protease inhibitor cocktail (Roche) and 4% Triton X-100. The lysate was cleared by centrifugation at 125,000xg for 1 hr at 4°C. The cleared lysate was added to 2 ml of equilibrated GSH-agarose beads and incubated for 3 hours at 4°C. The beads were pelleted and unbound protein was removed by aspiration. The beads were added to a 10 ml polyprep column (BioRad) and washed twice with 10 ml of Tris wash buffer (20 mM Tris pH7.5, 200 mM KCl, 5% glycerol, 0.5 mM TCEP, and 0.5% Triton X-100). The washed beads were resuspended in 10 ml Tris wash buffer and the protein was cleaved off of the beads with 0.1 mg GST-SENP2$^{365-589}$ protease overnight at 4°C. The cleaved protein was eluted out of the column into a 15 ml falcon tube by centrifugation then diluted with 20 mM Tris pH 7.5 so that the concentration of KCl was below 40 mM. The diluted protein was passed over a Q-sepharose column (0.5 ml/min), the detergent was washed away, and the protein was eluted off the column with a salt gradient from 40 mM to 1 M KCl. Peak fractions were pooled and desalted over two 5 ml Sephadex G-25 columns equilibrated in 20 mM Tris pH7.5, 200 mM KCl, 5% glycerol and 0.5 mM TCEP. The purified protein was aliquoted, plunged in $LN_2$, and stored at -80°C

### 2.2.3. SENP2 protease purification

In order to cleave the SUMO-tag off of the GST-SUMO-tagged proteins we purified recombinant, GST-tagged SENP2 protease. A pGEX vector containing the sequence for residues 365-589 of SENP2 protease was transformed into BL21(DE3) cells (Stratagene). Cells were grown in SuperBroth (Takara) + 100 μg/ml Amp in a 37°C incubator. A 250 ml overnight preculture was used to seed 4 liters of SuperBroth + Amp at an initial OD of 0.3 to 0.4. When the cells reached an OD between 0.7 and 0.8, protein expression was induced with 0.5 mM IPTG for 4 hours at 37°C. After 4 hours of expression the cells were harvested by centrifugation and washed once with 25 mM HEPES (pH7.4) and 200 mM KCl. The cells were broken in 25 mM HEPES (pH 7.4), 200 mM KCl, 10% glycerol, and 2 mM βME and the extract was centrifuged for 1 hour at 125,000 x g at 4°C. The cleared extract was incubated with 70 mg of swelled GSH-agarose beads (Sigma) for 1 hr at 4°C. The protein on the GSH-beads was washed with 20 ml of 25 mM HEPES (pH 7.4), 100 mM KCl, 10% glycerol, and 2 mM βME. The protein was eluted from the GSH-agarose beads with 25 mM HEPES (pH 7.4), 100 mM KCl, 10% glycerol, 2 mM βME, and 10 mM reduced GSH. The purified protein was diluted with HEPES buffer without salt so that the concentration of KCl was below 40 mM and then passed over a SP-sepharose column (GE). Protein was eluted off of the column using a salt gradient from 40 mM to 1 M KCl. Peak fractions were pooled and stored in 50% glycerol at -20°C. The protein concentration was determined by the Bradford protein assay[34].

## 2.3. Production of atlastin proteoliposomes

Purified recombinant GST- atlastin was reconstituted into synthetic liposomes to test for fusion.

### 2.3.1.1. Liposome preparation

Liposomes were made by the extrusion method as follows[35]. Unlabeled lipid mixes (POPC:DOPS, 85:15 mole ratio) and labeled lipid mixes (POPC:DOPS:Rhodamine-DPPE: 7-nitro-2,1,3-benzoxadiazol (NBD)-DPPE, 83:15:1.5:1.5 mole ratio) in chloroform were dried under a stream of $N_2$ gas followed by further drying in a vacuum for 30 min. The lipid films were then resuspended in A100 buffer (25 mM HEPES pH 7.4, 100 mM KCl, 10% glycerol, 2 mM BME, 1 mM EDTA) to a final total lipid concentration of about 10 mM. Large unilamelar vesicles (LUVs) were formed by 10 repeated freeze-thaw cycles in liquid N2 and room temperature water. Liposomes were formed by extruding the LUVs trough polycarbonate filters with 100 nm pore size (Avanti Polar Lipids). All the lipid mixes include trace amounts of $^3$H-lipid to determine the lipid concentrations of liposomes by liquid scintillation counting.

### 2.3.1.2. Atlastin reconstitution

GST-atlastin in 0.1% Triton X-100 (or 0.1% anapoe X-100) was reconstituted into both labeled and unlabeled 100 nm liposomes by the detergent assisted insertion method [35]. The protein in detergent was mixed with preformed liposomes at an effective detergent to lipid of about 1. The effective detergent to lipid ratio

($R_{eff}$) was determined by the following equation:

$$R_{eff} = D_{total} - \frac{D_{water}}{[lipid]}$$

**Equation 2-1: Detergent saturation of liposomes**

where $D_{total}$ is the total detergent concentration and $D_{water}$ is the monomeric detergent concentration (0.18 mM) in the presence of detergent[36]. The protein and lipid were mixed for 1 hour at 4°C. Detergent was removed by BioBeads® SM-2 adsorbant (BioRad) overnight at 4°C. Insoluble protein aggregates were pelleted by at 16,000xg for 10 min in a microcentrifuge cooled to 4°C. Final lipid and protein concentrations were determined by liquid scintillation counting and amido black protein assay[33], respectively. The liposomes sizes were confirmed by dynamic light scattering (DLS).

## 2.4. Measuring membrane fusion *in vitro*

### 2.4.1. *In vitro* fusion assay

Fusion assays were based upon the previously described[37] method used for analyzing SNARE-mediate fusion in vitro with the following modifications. Labeled and unlabeled populations of atlastin proteoliposomes (0.3 mM lipid each) were mixed in the presence of 0.5 to 1 mM GTP and brought to total volume of 45 µl with A100 buffer in well of 96-well Fluoronunc polysorp plate (Nunc). The samples in the plate were incubated at 37°C in fluorescent plate reader (Infinite m200, TECAN) for 5 min. To each well 5 µl of 50 mM $Mg^{2+}$ was added and NBD fluorescence was

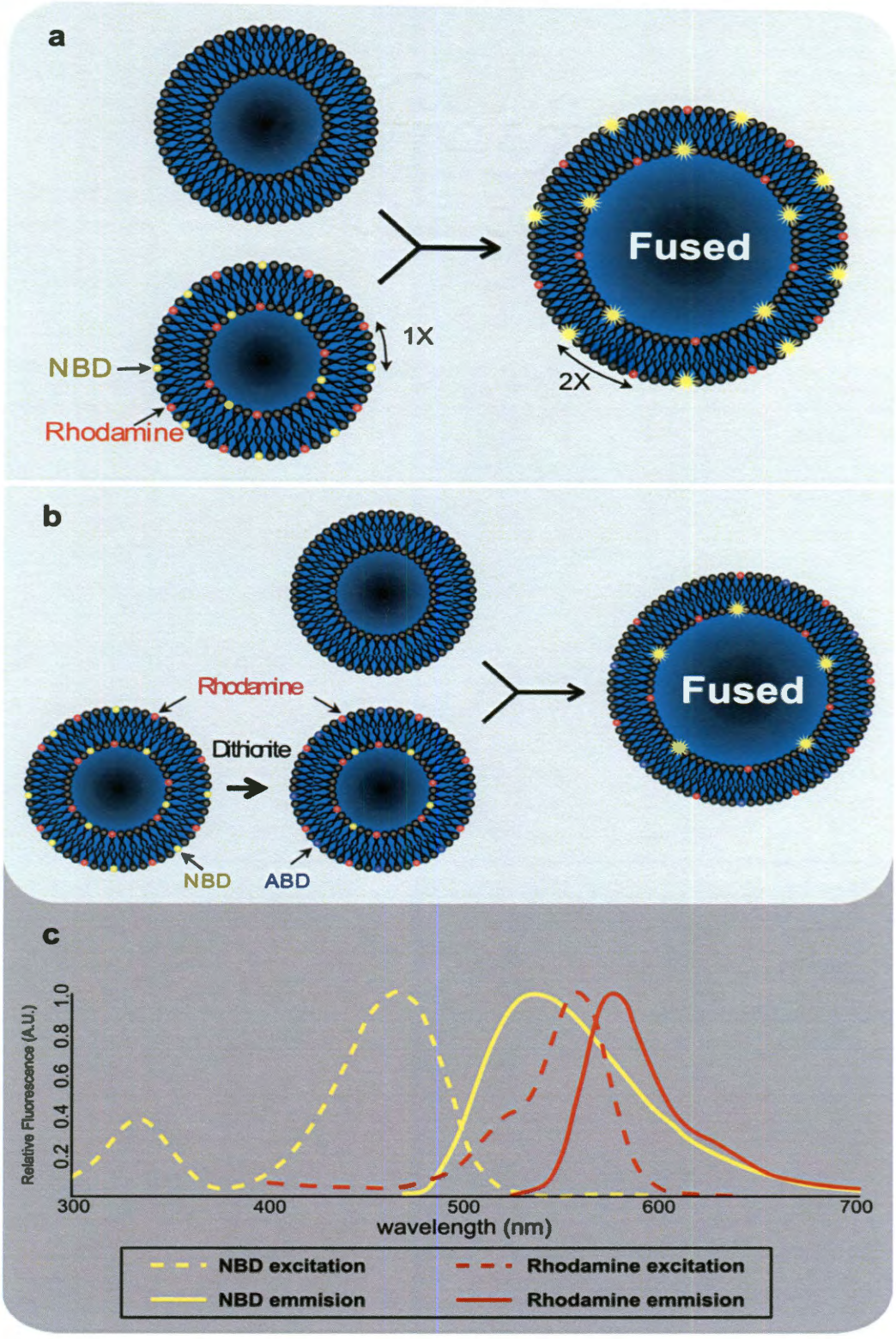


**Figure 2-1: In vitro fusion assay**

Cartoon depictions of a standard in vitro fusion assay (**a**) and inner-leaflet mixing assay (**b**). (**c**) Excitation and emission spectra of the FRET pair NBD and Rhodamine (SpecraViewer, Invitrogen). See text for details.

measured (excitation 460 nm, emission 538 nm, Figure2-1) at 1 min intervals for 60 min with 1 s shaking after every read. To determine the absolute NBD fluorescence 10 µl of 2.5% (w/v) n-dodecylmaltoside was added at 60 min. Data was normalized to percent total fluorescence.

The fusion measurement depends upon head-group labeled lipids in the labeled population of liposomes. The NBD and rhodamine labeled lipids are at a concentration (1.5 mole% of each) where the fluorescence of NBD is quenched by the rhodamine (Figure 2-1c). Under fusion conditions when liposomes fuse and mix their lipids the fusion of labeled liposomes with unlabeled liposomes dilutes the concentration of the labeled lipids 2-fold resulting in a relief of FRET and increase in NBD fluorescence (Figure 2-1a). We measure an increase in NBD fluorescence over time as a representation of membrane fusion.

The data are normalize to the maximum fluorescence after addition of detergent and are represented as a plot of percent of maximum fluorescence intensity (% of maximum) over time.

### 2.4.2. Inner-leaflet mixing

Inner-leaflet mixing (Figure 2-1b) is measured by reducing NBD to the non-fluorescent 7-amino-2,1,3-benzoxadiazol (ABD) with a membrane impermeable compound, dithionite (DTH). Labeled proteoliposomes are mixed in a 96 well fluoronunc polysorp plate and warmed to 37°C in TECAN Infinite M200 fluorescence plate reader. 100 mM dithionite in buffer (25 mM HEPES-KOH pH10,

10% Glycerol 100 mM KCl) is added to the wells before the initiation of fusion with $Mg^{2+}$. After addition of DTH does not result in further reduction in NBD signal the fusion reaction is performed the same as for the standard in vitro fusion assay. The NBD fluorescence is measured at 1 minute intervals and detergent (2.5% dodecylmaltoside) is added after 60 minutes to determine maximum fluorescence.

### 2.4.3. Dynamic light scattering

All the DLS data were acquired using Malvern Zetasizer Nano ZS and ZEN0040 cuvette. The scattering of light was recorded at 173°C (back scattering). The light intensity and the measurement time were automatically set by the software. To measure the dynamic change of liposome size, the experiments were performed at 37°C with 150 μM liposome in A100 buffer (100mM KCl, 25mM HEPES, 10% Glycerol, 1mM EDTA). Different nucleotides, Mg2+ or EDTA were added between measurements. The data are represented as Z-average size (diameter, nm).

### 2.4.4. Negative-stain transmission electron microscopy

Atlastin proteoliposomes (1 mM total lipid) were incubated with or without 2 mM GTP and 5 mM Mg2+ for 15 min at 37°C. EDTA was added to 10 mM concentration to stop liposome fusion following incubation. Samples were absorbed to bacitracin-treated carbon/formvar coated copper grids (Ted Pella), incubated for 3-5 min at room temp, and washed with 0.45 μM filtered 1% (w/v) ammonium molybdate. Samples were stained with 1% (w/v) ammonium molybdate for one

minute at room temperature and dried for at least 30 min. Stained samples were imaged on a JOEL 1230 high contrast transmission electron microscope operated at 80 keV.

## 2.5. GTPase activity measurements

### 2.5.1. Reversed-phase ion-paired high-performance liquid chromatography

Nucleotide species produced by atlastin were analyzed by reversed-phase ion-paired HPLC. GTPase reactions were setup by adding 0.5 mM GTP to 5 μM atlastin(1-422) brought up to a 350 μl volume with buffer A100. The reaction mixture was warmed to 37°C, 40 μl were removed for the 0 time point, and 5 mM $MgCl_2$ was added to start the reaction. For every time interval 40 μl were removed and added to a 0.5 ml microcentrifuge tube on wet ice containing 2.5 μl of 10% perchloric acid to precipitate the protein and stop the reaction. Following a 2 min incubation on ice the pH was raised by the addition of 1.75 μl of 4 M sodium acetate pH 4.0 and the precipitated protein was removed by centrifugation at 16,000xg for 5 minutes at 4°C. A Zorbax Eclipse XBD C-8 HPLC column (agilent) was equilibrated with running buffer comprised of 50 mM sodium phosphate pH 7, 10 mM tetra-n-butylammonium bromide (TBAB), and 7% acetonitrile. The nucleotide products were measured by running 20 μl of the cleared samples over the equilibrated column and measuring the absorbance at 254 nm. GTP, GDP, and GMP in buffer A100 were run over column as standards.

### 2.5.2. EnzChek® phosphate assay

GTPase activity measurements were done using an EnzChek® Phosphate assay kit (Invitrogen). A standard protocol for GTPase measurments involved mixing recombinant atlastin and atlastin mutants in a 150 µl reaction volume with 1 U/ml purine nucleoside phosphorylase (PNP), 200 µM 2-amino-6-mercapto-7-methylpurine riboside (MESG) and GTP in a transparent 96-well half-area plate. The plates were warmed to 37°C in a microplate reader (Tecan, Infinite M200) and 5 mM $Mg^{2+}$ was added to start the reaction. In the presence of inorganic phosphate, PNP catalyzes the conversion of MESG to ribose 1-phosphate and 2-amino-6-mercapto-7-methylpurine resulting in a spectrophotometric shift in absorbance from 330 nm to 360 nm (Figure2-2). The absorbance increase at 360 nm was measured in real-time every 30 seconds over 20 minutes.

GTPase assay data were analyzed by determining the initial rates of phosphate release as measured by the increase in absorbance at 360 nm and normalizing the data to a phosphate standard. For GTPase activity measured over a

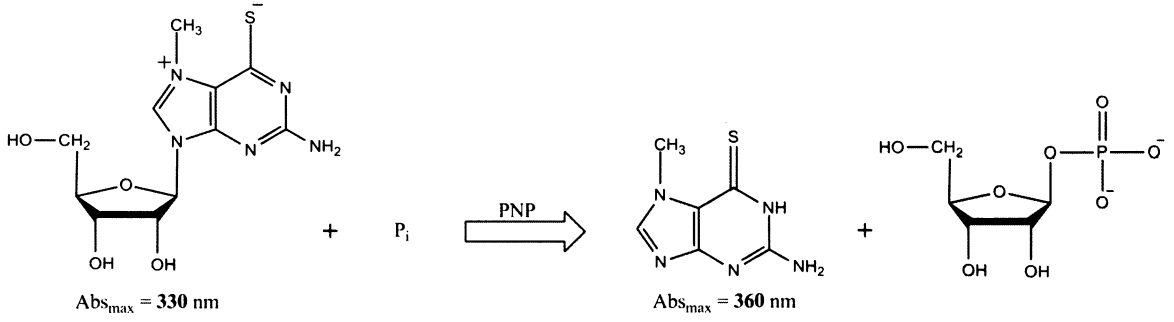


**Figure 2-2: EnzChek® Phosphate Assay**
A spectrophotometric shift from 330 nm to 360 nm during the conversion of MESG to 2-amino-6-mercapto-7-methyl-purine and ribose-1-phosphate by the enzyme PNP is used to measure inorganic phosphate produced in a GTPase reaction.

range of GTP concentrations the data was fit by the Michaelis-Menten equation to derive enzyme parameters.

$$v = \frac{V_{max} * [GTP]}{K_m + [GTP]}$$

**Equation 2-2: Michaelis-Menten equation**

## 2.6. Fluorescent nucleotide binding experiments

Equilibrium binding was done by measuring the change in fluorescence of N-methylanthraniloyl (mant)-nucleotides upon binding to soluble atlastin. In a black 96-well plate 1 μM mant-GTPγS or 1 μM mant-GDP was added to increasing amounts of purified GST-atlastin (1-422), GST-atlastin(1-422)K51A, or GST-atlastin(1-422)R48E. The mant fluorescence (λEx=366 nm, λEm=435 nm) was measured in a TECAN infinite M200 fluorimeter every 2 minutes for 20 minutes and averaged. The absolute fluorescent intensities were plotted versus protein concentration and curve fitted to determine the equilibrium dissociation constants ($K_d$) according to the following equationuation[38]:

$$F = F_{min} - (F_{max} - F_{min}) \frac{A_0 + B_0 + K_d - \sqrt{(A_0 + B_0 + K_d)^2 - 4A_0B_0}}{2B_0}$$

**Equation 2-3: Curve fiting equation for nucleotide equilibrium binding.**

where $F_{min}$ is the fluorescence minimum, $F_{max}$ is the fluorescence maximum, $A_0$ is the concentration of protein in μM, $B_0$ is the concentration of mant-GTPγS in μM and $K_d$ is the equilibrium binding constant in μM. A global value of $F_{max}$ from was used in all three curve fits. Measurements were carried out with at least two independent preparations of each protein.

## 2.7. Analytical ultracentrifugation

Analytical ultracentrifugation experiments were performed using a Beckman Optima XLA analytical ultracentrifuge. Buffers used were 20 mM Tris pH 7.5, 200 mM KCl, 0.5 mM TCEP, 5%(w/v) glycerol. Sedimentation velocity experiments were carried out with 3.5 μM protein and 20 μM nucleotide in cells assembled with 12 mm, 2-channel aluminum centerpieces. Water was used in the reference channel of each cell. Experiments were carried out at 50,000 or 55,000 rpm in an AN60 rotor at 20°C. Intensity at 235 nm versus radial position was measured at 4 min intervals for 4 to 5 hours. All data analysis was done using Ultrascan II[39]. The intensity data were converted to pseudo-absorbance using water as the reference channel. Time-invariant and radial-invariant noise was fit to the data by two-dimensional spectral analysis (2DSA) and subtracted from each data set. The edited data were analyzed using the enhanced van Holde-Weischet module in Ultrascan to determine diffusion-corrected $S_{W,20}$ values for each samples. The data were further analyzed to determine frictional ratios and molecular weights by fitting the data to a model by least squares methods using parameters describing the sedimentation and diffusion of the samples.

Chapter 3

# Drosophila Atlastin Mediates Membrane Fusion

## 3.1. In vivo evidence that atlastin is involved in endoplasmic reticulum membrane fusion

Our collaborator Andrea Daga (E. Medea Scientific Institute, Italy) initially suggested to the McNew lab that atlastin may be directly responsible in ER membrane fusion. Work performed in their lab using the model organism *Drosophila melanogaster* supported their hypothesis that atlastin plays a direct role in ER fusion. They found that atlastin, an integral membrane GTPase, is localized to the ER in flies without any colocalization with golgi markers[40]. Atlastin was shown to form a homooligomer in immunoprecipiation assays[40]. And as shown below misexpression of atlastin results in abnormal ER morphologies.

### 3.1.1. Depletion of atlastin results in ER fragmentation

To gain insight into the function of atlastin, the consequences of downregulating the expression of atlastin in Drosophila by in vivo RNAi was examined. The Daga lab generated UAS-atlastin-RNAi transgenic flies, whose expression could be controlled using the Gal4/UAS system[41]. Loss of atlastin in muscle and neurons resulted in severely undersized and fragmented ER profiles in contrast to control neuron ER profiles (Fig. 3-1)[40]. EM analysis showed analogous shortened, fragmented ER profiles in atl1 null mutant neurons[7] (Fig. 3-1). These results indicate that the ER is fragmented in direct response to a loss of ER membrane fusion and atlastin plays a close role in this process.

The functional consequences of these morphological changes in ER structure were examined by fluorescence loss in photobleaching (FLIP) experiments. Loss of a fluorescent marker from a region of a cell upon repeated photobleaching of a different region indicates continuity between the two regions. FLIP experiments targeting GFP-KDEL[42,43] were used to assess whether fragmentation in atlastin-RNAi tissue resulted in discontinuity of normally interconnected ER elements. Unlike in control muscle where loss of GFP-KDEL fluorescence was homogeneous, repetitive photobleaching of GFP-KDEL in tubulin-Gal4/+; UAS-atlastin-RNAi/+ muscles produced regions of unbleached fluorescence (Fig. 3-1)[40], indicating that in these areas the ER network lacked its typical continuity. These data reinforced the EM observations demonstrating that removal of atlastin results in ER fragmentation.

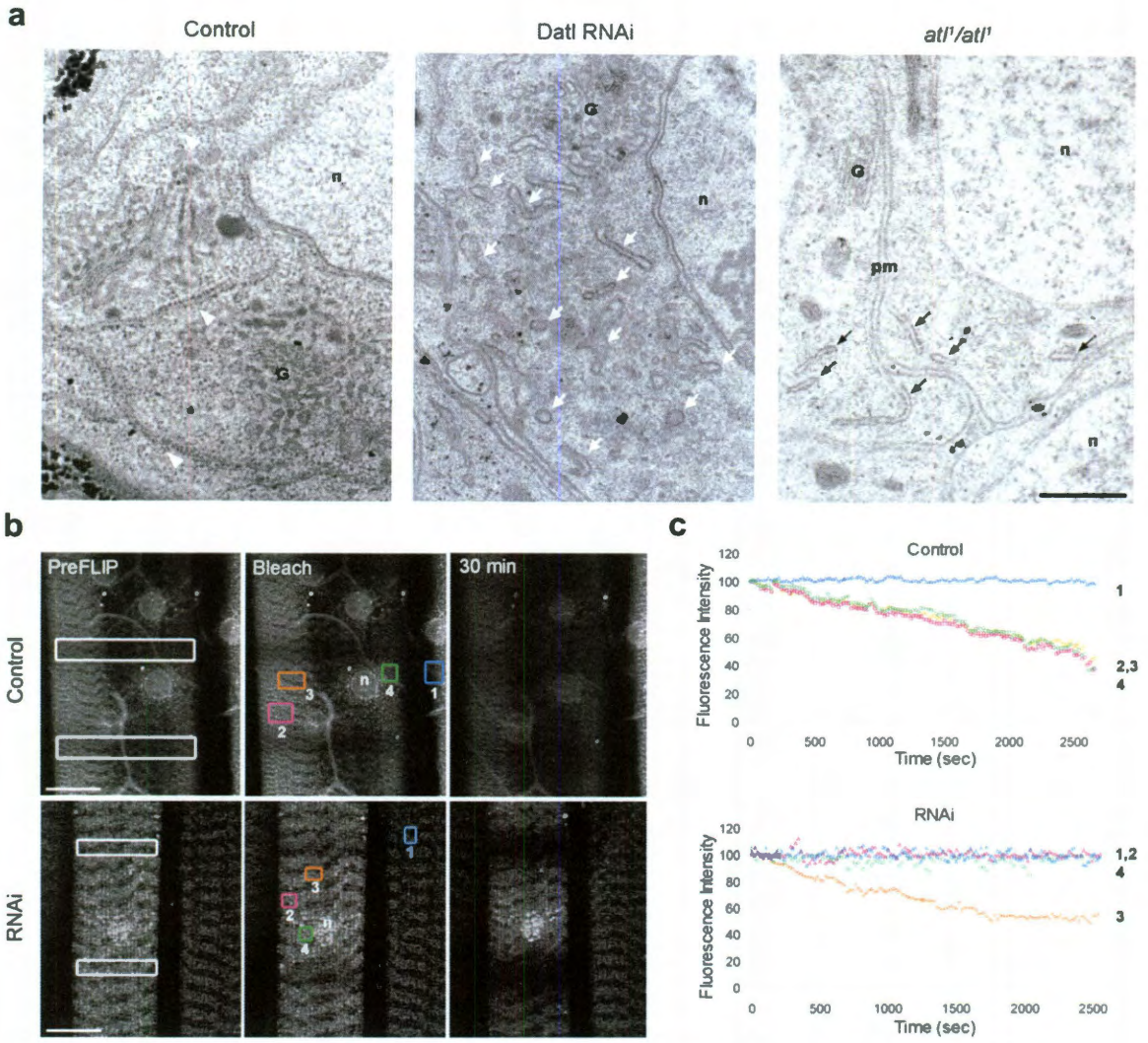


**Figure 3-1: Atlastin depletion in flies results in shortened, fragmented ER**

(**a**)TEM images of motor neurons show normal tubular ER(arrowheads) in WT flies and fragmented ER (arrows) in atlastin RNAi and atlastin null flies (Scale bar, 0.5 μm; G, golgi; n, nucleus; pm, plasma membrane) (**b**)FLIP experiments on fly muscle cells expressing GFP-KDEL that were repeatedly photobleached (white outlines) while fluorescence intensity was measured in adjacent regions (colored outlines, scale bar, 20 μm). (**c**) Kinetic graphs of FLIP experiments. Experiments performed in the lab of Andrea Daga.

### 3.1.2. Overexpression of atlastin results in ER expansion

Since reduction in atlastin levels produced ER fragmentation, a D42-Gal4/+;UAS-atlastin-myc/+ fly line overexpressing atlastin in the brain was constructed to determine whether atlastin was directly involved in fusion and would result in excessive ER fusion. EM analysis of D42-Gal4/+;UAS-atlastin-myc/+ brains revealed that atlastin overexpression results in an abnormal ER morphology. Normal tubular ER profiles were absent in atlastin overexpressing motorneurons where ER membranes formed expanded cisternae (Fig. 3-2)[40]. This expansion of ER elements is consistent with an increase in membrane fusion and suggested that atlastin itself could directly mediate bilayer merger.

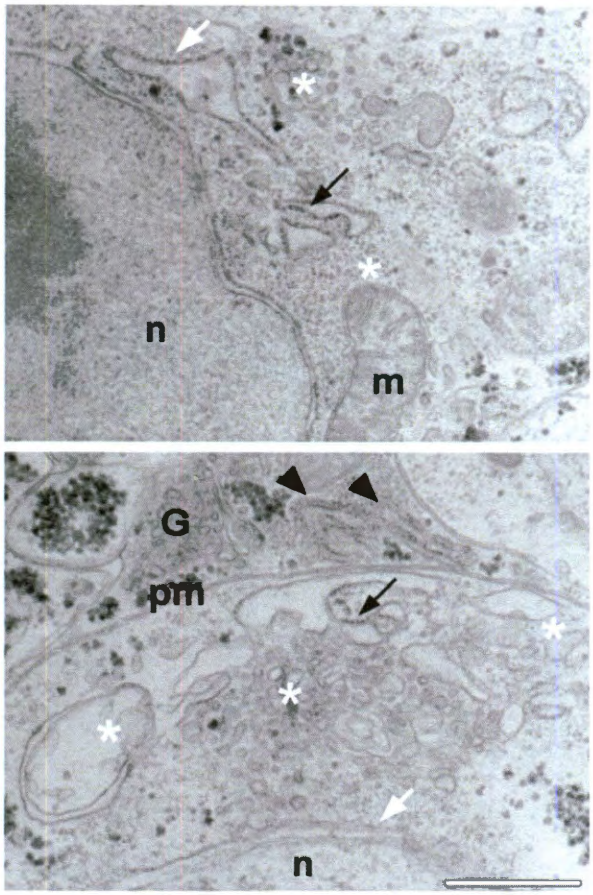


**Figure 3-2: Transmission electron micrographs reveal cells overexpressing atlastin have expanded, dilated ER.**
TEM analysis of D42-Gal4/+;UAS-atlastin-myc/+ motor neurons show that overexpressing Atlastin exhibit results in an expanded ER(asterisks) and nuclear envelope (white arrows). Note a non-overexpressing neuron with normal tubular ER morphology (black arrowheads). Scale bar, 0.5 mm. m, mitochondrion; n, nucleus; pm, plasma membrane. Black arrows denote ribosomes. Experiments performed in the Daga lab.

## 3.2. In vitro measurements of atlastin mediated fusion

The in vivo experiments performed by our collaborators suggested that atlastin may play a direct role in ER membrane fusion. To determine whether this is true we made purified recombinant GST-tagged *Drosophila* atlastin from *E. coli* (BL21) cells. The recombinant protein was purified over a glutathione (GSH)-column and eluted off the column with free glutathione. Since atlastin is a membrane protein it has to be purified in detergent. Initial attempts to purify atlastin in mild octyl-glucoside detergents resulted in precipitation of the protein. We instead purified the protein in low amounts of Triton X-100. To test the fusion activity of purified recombinant atlastin we needed to reconstitute the protein into the lipid bilayer of synthetic liposomes. The need to purify atlastin in Triton X-100 made it difficult to reconstitute the protein into liposomes by traditional dilution-dialysis methods[37] and necessitated the use of a different method of protein reconstitution.

Atlastin was reconstituted into preformed 100 nm liposomes by detergent-assisted insertion[44] followed by detergent removal with BioBeads absorbant SM-2. The resultant atlastin proteoliposomes were assayed for fusogenic activity using three techniques.

### 3.2.1. Atlastin promotes lipid mixing

First, an in vitro fusion assay made standard in studies of SNARE proteins[37] was used to assess whether atlastin could promote membrane fusion. Recombinant

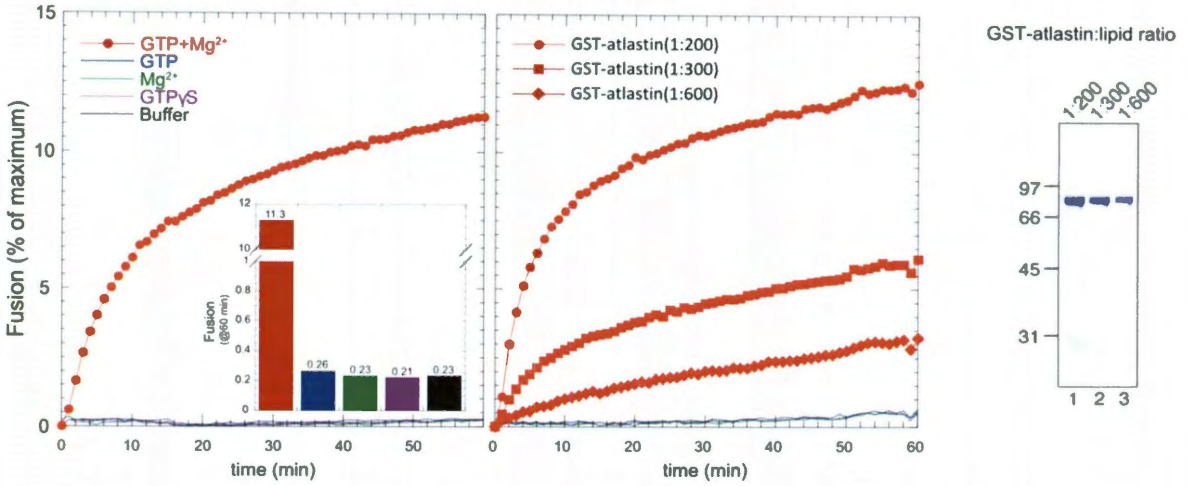


**Figure 3-3: Atlastin proteoliposomes undergo fusion in the presence of GTP and $Mg^{2+}$.** (**Left**)GST-atlastin drives fusion in vitro. Kinetic fusion graph of unlabeled fly atlastin proteoliposomes fused with equimolar fluorescently labeled fly atlastin proteoliposomes. NBD fluorescence was measured at 1 minute intervals and 2.5% dodecylmaltoside was added at 60 minutes to determine maximum fluorescence. Fusion is represented as a percent of maximum fluorescence intensity (% of maximum) over time. The extent of fusion at 60 minutes is shown as a histogram inset. (**Middle**) Surface density concentration dependence of fly atlastin-mediated fusion. Surface density is represented as a protein:lipid molar ratio. (**Right**) Coomassie-stained gel of proteoliposomes analyzed in middle panel run on SDS-PAGE gel. Data by Song Liu (McNew Lab)

GST-atlastin was reconstituted into two populations of preformed liposomes[44]. Acceptor proteoliposomes containing unlabeled lipids and donor proteoliposomes contained these lipids as well as equimolar amounts of NBD and rhodamine head-group labeled lipids. NBD and rhodamine form a FRET pair and fusion is measured as an increase in NBD fluorescence (Figure2-1) over time as lipid mixing between donor and acceptor proteoliposomes dilutes the fluorescence probes in the newly merged membrane. Lipid-mixing assays were carried out by mixing equimolar donor and acceptor proteoliposomes and then adding GTP and $Mg^{2+}$ to trigger fusion (Fig. 3-3). GST-Atlastin proteoliposomes in the presence of $Mg^{2+}$ and GTP drives robust fusion that is completely dependent on GTPase activity (see chapter 4). The fusion observed is dependent upon concentration of protein in the liposomes (Figure3-3).

### 3.2.2. Atlastin promotes inner-leaflet mixing

The in vitro fusion assay measures total lipid mixing and does not discriminate between full fusion and outer-leaflet mixing. The possibility remained that the lipid mixing observed was due only to aggregation of liposomes and merging of the outer leaflets alone. To test if full fusion occurs between atlastin proteoliposomes I measured the extent of inner-leaflet mixing. This is done by preferentially quenching the NBD in the outer-leaflet of the atlastin proteoliposomes with the membrane impermeable reducing agent dithionite (DTH) (Figure 2-1). Labeled atlastin proteoliposomes treated with DTH show about a 3-fold decrease in NBD signal (Figure 3-4). After Mg2+ and GTP addition to the DTH-treated atlastin proteoliposomes lipid mixing still occured as represented in an increase in NBD fluorescence (Figure 3-4). This suggests that atlastin promotes full fusion.

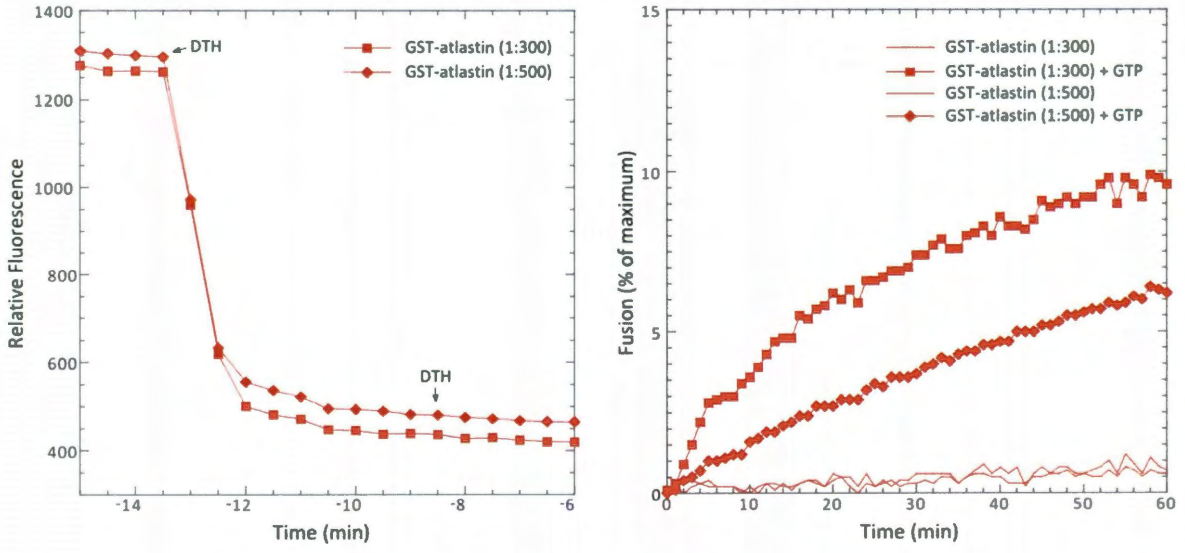


**Figure 3-4: Atlastin promotes the full fusion of liposomes.**
Labeled atlastin proteoliposomes are treated with 100 mM dithionite (DTH) 13.5 and 8.5 minutes before the initiation of fusion with GTP and $Mg^{2+}$. The relative fluorescence decreases (**left**) as the NBD in the outer-leaflet of the liposomes is quenched with DTH. NBD-labeled headgroups protected from DTH in the inner-leaflet of the liposomes show increased fluorescence (**right**) as the liposomes fuse.

### 3.2.3. Atlastin promotes aggregation of liposomes

A second indirect method of measuring fusion was used to support the lipid mixing results as this was the first time that a Dynamin-like GTPase was shown to be involved in membrane fusion. The hydrodynamic diameter of atlastin proteoliposomes was analyzed by dynamic-light scattering (DLS). The average diameter of atlastin proteoliposomes was about 125 nm and the diameter increased after the addition of GTP and $Mg^{2+}$ consistent with a role for atlastin in membrane fusion. The average diameter of the liposomes increased until the GTPase activity was quenched by the sequestering of free $Mg^{2+}$ with the addition of the metal chelating compound EDTA (Figure 3-5). After the GTPase activity was quenched the size of the atlastin proteoliposomes decreased to an average diameter of about 165nm (Figure 3-5). These data suggest that under these conditions there may be some aggregation of GST-atlastin proteoliposomes that may or may not lead directly to fusion. The aggregates were broken apart by the addition of EDTA and the average size settled at an average diameter consistent with a doubling in the surface area of the liposomes. DLS measurements support the lipid mixing assay and suggest that GST-atlastin proteoliposomes undergo on average of one round of fusion.

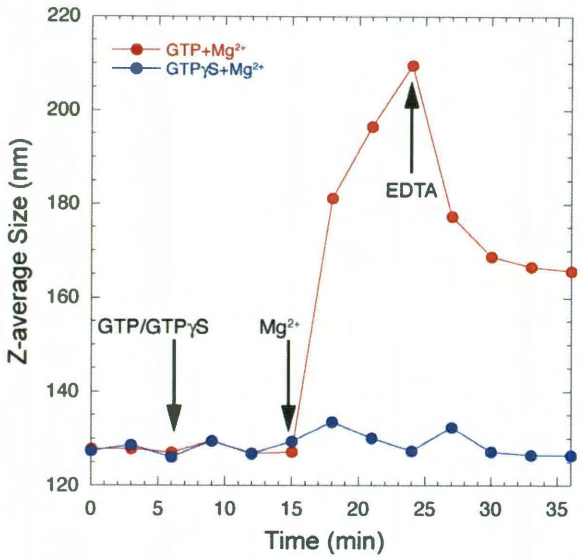


**Figure 3-5: Atlastin proteoliposome size measurements**

DLS size measurements taken over 3 minute intervals. Atlastin proteoliposome size increases after the addition of GTP and $Mg^{2+}$, but not GTPγS. Data by Song Liu.

### 3.2.4. Atlastin promotes an increase in liposomes diameter

Lastly, a more direct method of analyzing liposome fusion is to image the liposomes by microscopy. The diameter of the liposomes is roughly 100 nm which is below the resolution of light microscopy. Thus, I imaged the atlastin proteoliposomes by electron microscopy. Atlastin proteoliposomes were incubated in buffer or with 5 $Mg^{2+}$ and 2 mM GTP for 15 min at 37°C. Fusion was stopped by the addition of 10 mM EDTA following incubation. The liposomes were absorbed to bacitracin-treated grids and negative-stained with ammonium molybdate. The liposomes are modestly deformed by the negative-staining protocol; however it is

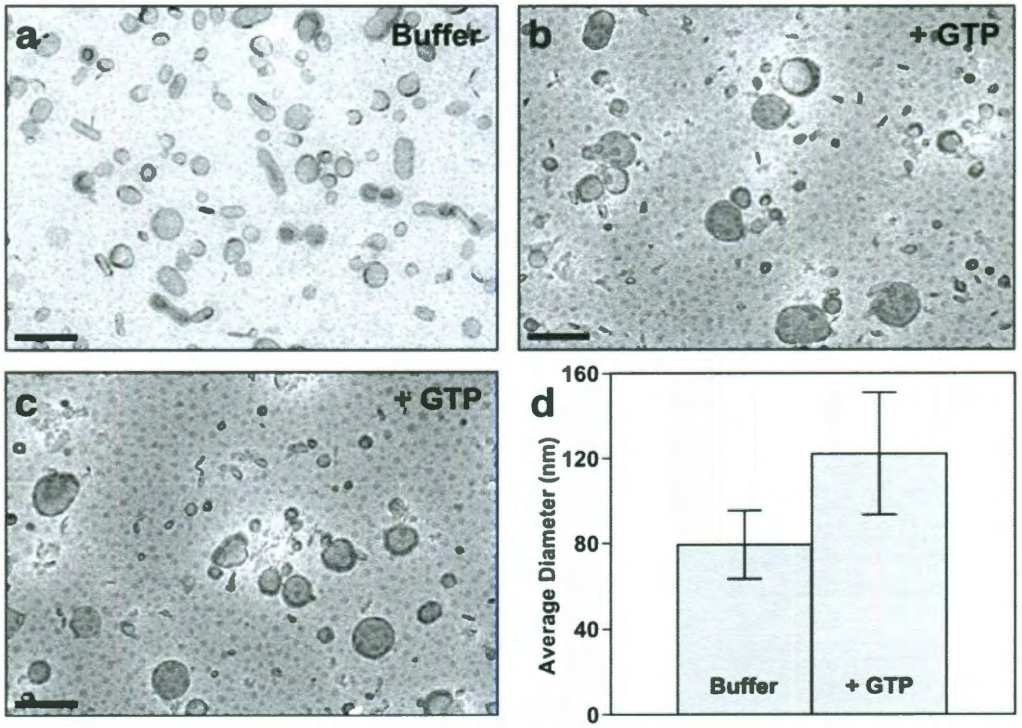


**Figure 3-6: Transmission electron microscopy of negative-stained atlastin proteoliposomes.**
(**a**) Unfused atlastin proteoliposomes incubated without GTP. 12,000x magnification. (**b** and **c**) Fused atlastin proteoliposomes incubated with 2 mM GTP. 10,000x magnification. (**d**) The atlastin proteoliposomes treated with GTP prior to imaging showed a greater average diameter (~122 nm) relative to the untreated proteoliposomes (~79 nm). Scale bars, 200 nm.

clear the liposomes have an increased diameter in the samples with GTP (Figure 3-6).

Of note is that the liposomes are spherical (Figure 3-6) after GTP addition, the same conditions where lipid mixing is observed. This is a clear distinction from dynamin which form tubules out of liposomes in the presence of GTP[45]. Atlastin is a distant member of the dynamin superfamily of GTPases.

## 3.3. Conclusions

These in vitro results coupled with the in vivo evidence from our collaborators convinced us that atlastin is able to fuse membranes and is directly responsible for the fusion of ER membranes.

Concurrent with the publication of our results an article[14] from the lab of Tom Rapoport (Harvard Medical School) came to the same conclusion, i.e. that atlastin is the GTPase responsible for ER membrane fusion. They showed that HeLa cells that are atlastin depleted have long unbranched ER tubules. Additionally, they used an assay that they had previously established[12] wherein they are able to reform ER networks from microsomes extracted from *Xenopus* eggs. This in vitro ER network formation is inhibited by a pan-atlastin antibody[14].

# Chapter 4

# Atlastin oligomerization

## 4.1. Atlastin forms homooligomers in vivo

Atlastin is responsible for the homotypic fusion of ER membranes. Homotypic fusion is the fusion of two membranes that are indistinguishable from each in their protein and lipid content. Atlastin must be present in both bilayers to promote fusion (data not shown) ergo, atlastin must self-associate to form homo-oligomers prerequisite to promoting fusion.

Most large GTPases, like atlastin, form higher order oligomeric structures and human Atlastin-1(Atl1) has been shown to self-associate in vivo. In vitro analysis of the N-terminal cytoplasmic domain of Atl1[46] revealed that it is a monomer that shifts to a size consistent with a dimer in the presence of nonhydrolyzable GTP[46]. However, immunoprecipitated full-length Atl1 migrates as an apparent homotetramer by gel filtration[23], as does Atl2 and Atl3[26]. Either the

transmembrane segments and the C-terminal tail influence oligomerization, or the immunoprecipitated material from detergent extracts contained additional mass not attributable to atlastin. Attempts to identify heteroligomeric complexes have met with mixed results. Endogenous Atl1 and Atl2 do not coprecipitate other atlastins; however, mixed heteroligomeric complexes can be coprecipitated when atlastins are overexpressed[26].

In vivo data from the Daga Lab confirms that *Drosophila* atlastin is also capable of homooligomerization. They performed co-immunoprecipitation of atlastin-myc and atlastin-HA coexpressed in HeLa cells and demonstrated the self-association of atlastin molecules[40]. Additionally, they prepared microsomes from HeLa cells separately transfected with atlastin-myc or atlastin-HA. When anti-myc antibodies were used to precipitate atlastin-myc harboring vesicles, atlastin-HA was recovered in the pellet. Fractionation of cleared cell homogenates showed that atlastin and the ER resident integral membrane protein calnexin partitioned exclusively to the membrane fraction while the ER-lumenal protein PDI remained in the soluble fraction. These experiments demonstrated that under these lysis conditions atlastin associated with membranes and atlastin binding occurred between distinct vesicles[40].

## 4.2. Atlastin dimerization

In vivo methods show oligomerization of atlastin but do not clearly show the number of subunits in the atlastin homooligomer. I purified two soluble forms of

atlastin, atlastin(1-422) and atlastin (1-328), to be able to work with the recombinant protein in the absence of detergent so that I didn't get any contribution in size from detergent micelles. I expressed and purified fly atlastin(1-422) which is lacking the 2 TMDs and the c-terminal cytoplasmic domain. The GST-SUMO-tagged atlastin(1-422) was made by tandem purification over a GSH-column followed by ion-exchange. The GST-SUMO-tag was cleaved off by SENP2 protease prior to purification by ion exchange.

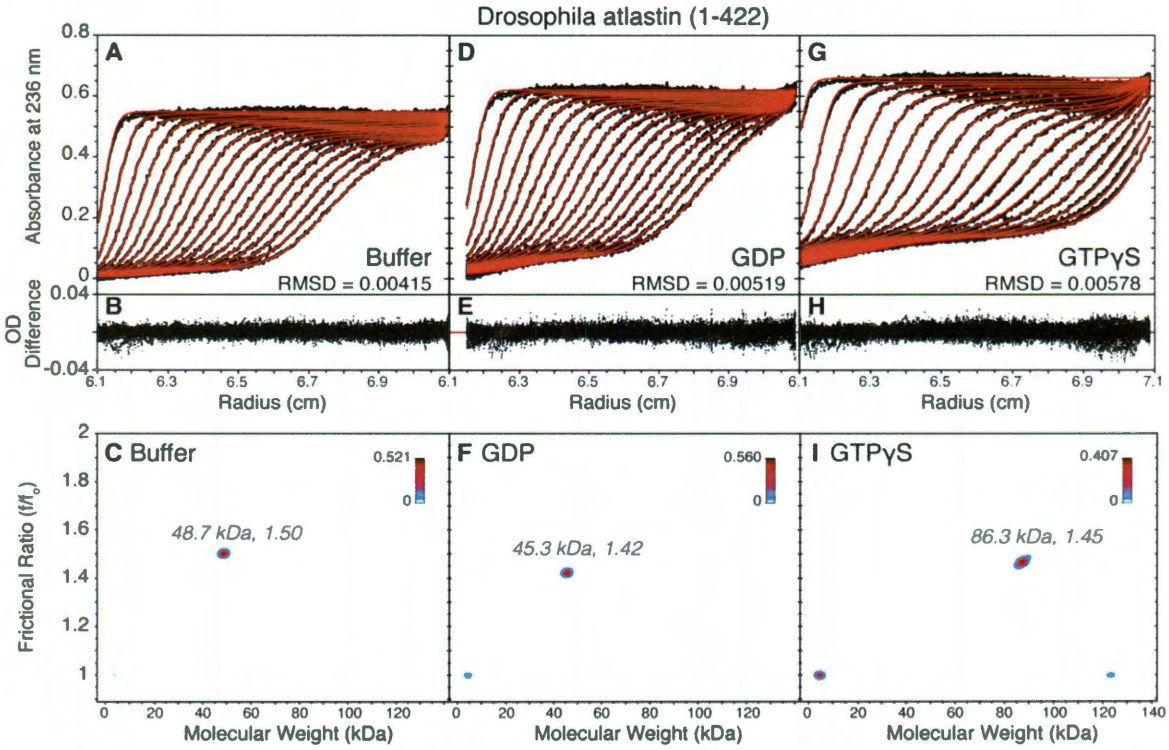


**Figure 4-1: Sedimentation velocity analysis of atlastin (1-422)**
(**A**,**D**, and **G**) Edited data plots (black) and the best fit models (red) of sedimentation velocity experiments with atl1-422 in the presence of buffer only, 20 μM GDP, or 20 μM GTPγS. Every 2nd and 3rd radial scan is excluded for ease of viewing. Residuals (**B**, **E**, and **H**) and Pseudo-3D plots (**C**, **F**, and **I**) of the respective species best describing the fitted models show that atlastin(1-442) is monomeric in buffer and 20 μM GDP, 48.7 kDa and 45.3 kDa respectively. In the presence of 20 μM GTP atlastin (1-422) forms a homo-dimer, 86.3 kDa.

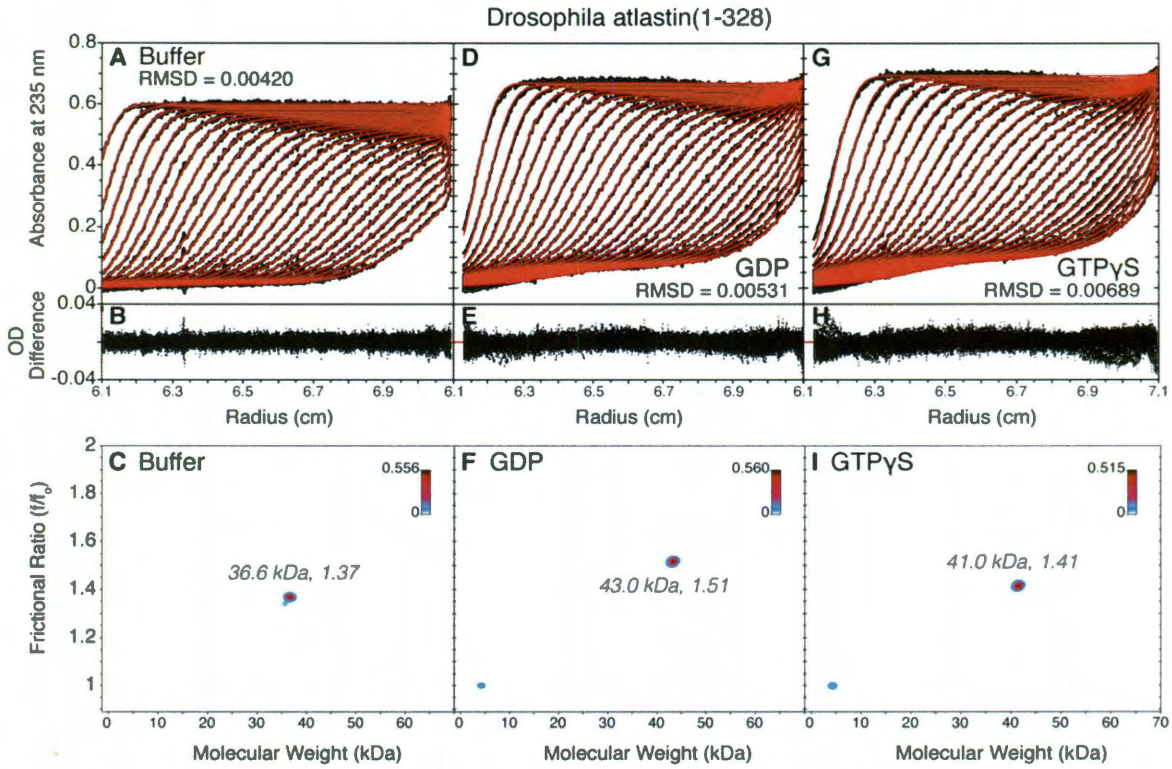


**Figure 4-2: Sedimentation velocity analysis of atlastin (1-328)**

**A**,**D**, and **G**) Edited data plots (black) and the best fit models (red) of sedimentation velocity experiments with atl1-422 in the presence of buffer only, 20 μM GDP, or 20 μM GTPγS. Every 2nd and 3rd radial scan is excluded for ease of viewing. Residuals (**B**, **E**, and **H**) and Pseudo-3D plots (**C**, **F**, and **I**) of the respective species best describing the fitted models show that atlastin(1-442) is monomeric in buffer, 20 μM GDP and, 20 μM GTP; 36.6 kDa, 43.0 kDa, and 41.0 kDa respectively.

To address the question of oligomerization directly, we measured the molecular mass of atlastin (1-422) and atlastin (1-328) by analytical ultracentrifugation (AUC)[47]. Figures 4-1 and 4-2 show the results of velocity sedimentation experiments for these proteins. The edited radial scans fitted with a genetic algorithm analysis using Ultrascan II[39] to determine the sedimentation and frictional coefficients of protein migrating through the cells in buffer only, 20 μM GDP or μM GTPγS. When sedimentation and frictional coefficients were known, molecular weights were able to be calculated. Atlastin (1-422) showed molecular weights of 48.7 (Apo), 45.3 (GDP) and 86.3 (GTPγS) kDa respectively (Figure 4-1). The predicted monomer molecular weight of atl (1-422) is 49,317 Da strongly

suggesting that both the apo and GDP-bound protein is monomeric while the GTPγS-bound protein forms a dimer. A similar analysis with atl (1-328) produces a different result. In this case, all three species (apo, GDP and GTPγS) migrate at a size most consistent with a monomer molecular weight (36.6, 43.0, and 41.0 kDa, respectively). The predicted monomer molecular weight of atl (1-328) is 37,243 Da. These data suggest that the middle domain 3HB of atlastin is important to form or stabilize dimers.

Taken together, GTPase activity measurements and molecular weight

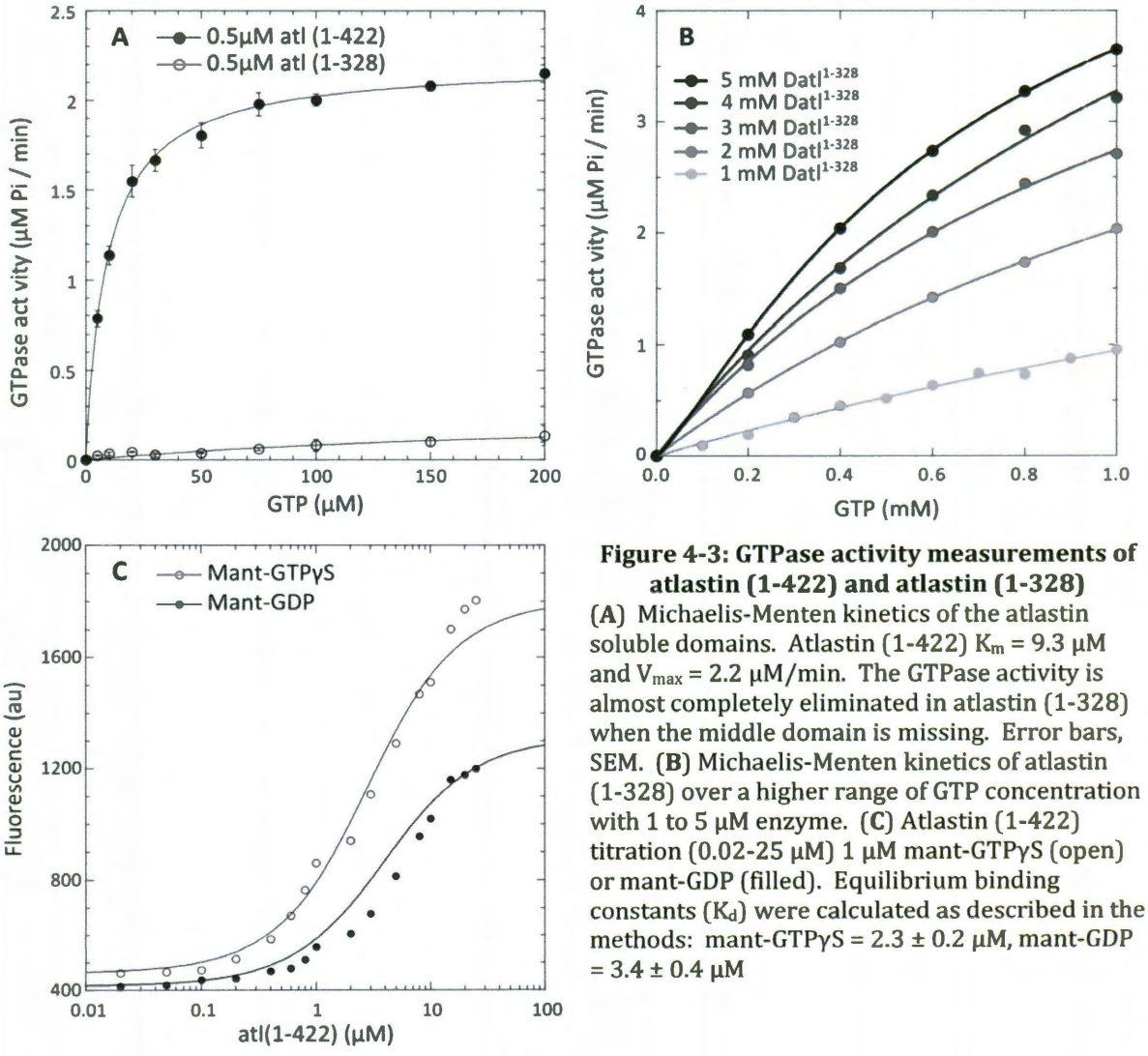


**Figure 4-3: GTPase activity measurements of atlastin (1-422) and atlastin (1-328)**
**(A)** Michaelis-Menten kinetics of the atlastin soluble domains. Atlastin (1-422) $K_m$ = 9.3 μM and $V_{max}$ = 2.2 μM/min. The GTPase activity is almost completely eliminated in atlastin (1-328) when the middle domain is missing. Error bars, SEM. **(B)** Michaelis-Menten kinetics of atlastin (1-328) over a higher range of GTP concentration with 1 to 5 μM enzyme. **(C)** Atlastin (1-422) titration (0.02-25 μM) 1 μM mant-GTPγS (open) or mant-GDP (filled). Equilibrium binding constants ($K_d$) were calculated as described in the methods: mant-GTPγS = 2.3 ± 0.2 μM, mant-GDP = 3.4 ± 0.4 μM

analysis by analytical ultracentrifugation suggests that the N-terminal cytoplasmic domain of Drosophila atlastin can dimerize in the presence of GTP and that nucleotide binding promotes a conformation that requires the middle domain for stable oligomerization.

GTPase activity measurements (Figure4-3) and soluble domain inhibitor results (see chapter 6) suggest that the "middle domain" of atlastin may be important for oligomerization. Atlastin(1-328) does not form a dimer and shows weak enzymatic properties. Michaelis-Menten kinetics could not be fitted for atlastin (1-328) at these protein and GTP concentrations as opposed to atlastin (1-422) (Figure 4-3a). At higher concentrations of enzyme and GTP the soluble GTPase domain alone shows greater GTPase activity and can be weakly fit by the Michaelis-Menten equation (Figure 4-3b).

## 4.3. Conclusions

Recently, two reports detailing the X-ray structure of the N-terminal

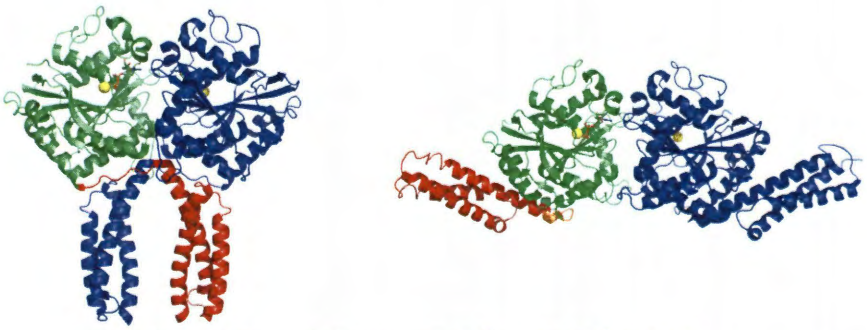

**Figure 4-4: Crystal structures of human atlastin 1**
Crystal structures of human atlastin-1 reveal to forms of atlastin when bound to nucleotide. Form 1 (3Q5D) represents a post-fusion (cis) dimer. Form 2 (3Q5E) represents a pre-fusion (trans) dimer. Green GTPase domain, orange linker, red 3-helix bundle.

cytoplasmic domain of human Atlastin-1 were published[46,48]. These data provide important insights into both the biochemical properties and potential fusion mechanism of atlastin. The large GTPase domain shares significant structural similarity to human guanylate binding protein-1 (hGBP1)[49] and the "middle domain" folds into an antiparallel 3-helix bundle (3HB) that would connect the GTPase domain to the tandem transmembrane segments. The GTPase domain is connected to the 3HB by a flexible linker. Both groups identified two crystal forms of Atlastin-1 (1-446) differing by the position of the 3HB relative to the GTPase domain. Crystal form 1[46] (Figure4-4) would likely position the transmembrane domains in a "post-fusion" conformation[48], while crystal form 2 probably represents a pre-fusion structure. All of the current structures contained bound GDP although attempts were made to bind nonhydrolyzable GTP analogs like GTPγS or GMPPNP.

Biochemical analysis of the Atl1 (1-446) N-terminal cytoplasmic domain showed that GTPase activity of the wildtype human protein was comparable to our Drosophila protein (5.33 μM Pi/ min / μM enzyme for Atl1 (1-446) vs. 4.4 for μM Pi/ min / μM enzyme for atl (1-422)) and that GTP promoted dimerization measured by small angle X-ray scattering (SAXS)[46] or analytical ultracentrifugation (AUC)[48]. Additionally, both groups measured dimerization by gel filtration in the presence of GDP that yielded different outcomes. Tom Rapoport's group[48] identified atlastin dimers in the presence of GDP, while Byrnes and Sondermann[46] found only monomers with GDP. SAXS analysis also supported a monomer in the presence of GDP. This apparent discrepancy may be explained by different experimental conditions such as protein or nucleotide concentration. We detected only

monomeric atl (1-422) with GDP and equilibrium binding data (Figure4-3c) suggest that the concentration of GDP used in our analysis should be sufficient for atl (1-422) to bind the GDP.

Chapter 5

# Atlastin Mediated Membrane Fusion requires GTPase hydrolysis

## 5.1. Characterization of GTPase activity

Atlastin belongs to the superfamily of dynamin-like GTPases[50]. It has been established that ER membrane fusion requires GTP[12] and that atlastin is a GTPase directly responsible for fusion. Additionally, many of the HSP causing mutation lie in the GTPase domain of atlastin (Table5-1) While it is clear the GTP domain of atlastin is essential to its function in promoting ER membrane fusion we know very little regarding the enzymatic properties of atlastin and it remains unclear how GTP binding and hydrolysis is translated into fusion.

To address these issue, we measured Michaelis-Menten kinetics for full-length GST-atlastin in detergent and reconstituted into proteoliposomes using a coupled enzymatic assay that quantifies inorganic phosphate production. This assay

includes purine nucleoside phosphorylase (PNP) which consumes the free phosphate released by the GTPase activity of atlastin and couples this consumption with a detectable output by phosphorylating another substrate, MESG, producing ribose-5-phosphate and 2-amino-6-mercapto-7-methylpurine which has measurable absorbance at 360 nm (Figure 2-2). Using this coupled assay I can detect continuous production of phosphate from GTPase activity. I insured that quantifying inorganic phosphate production was a reliable measure of GTPase activity by examining all of the guanine nucleotide reaction products by HPLC (Figure 5-1a) since GBP1, another large GTPase family member similar in sequence to atlastin, is capable of sequentially cleaving GTP to GMP[49].

To determine the GTPase activity of the atlastin in detergent and in

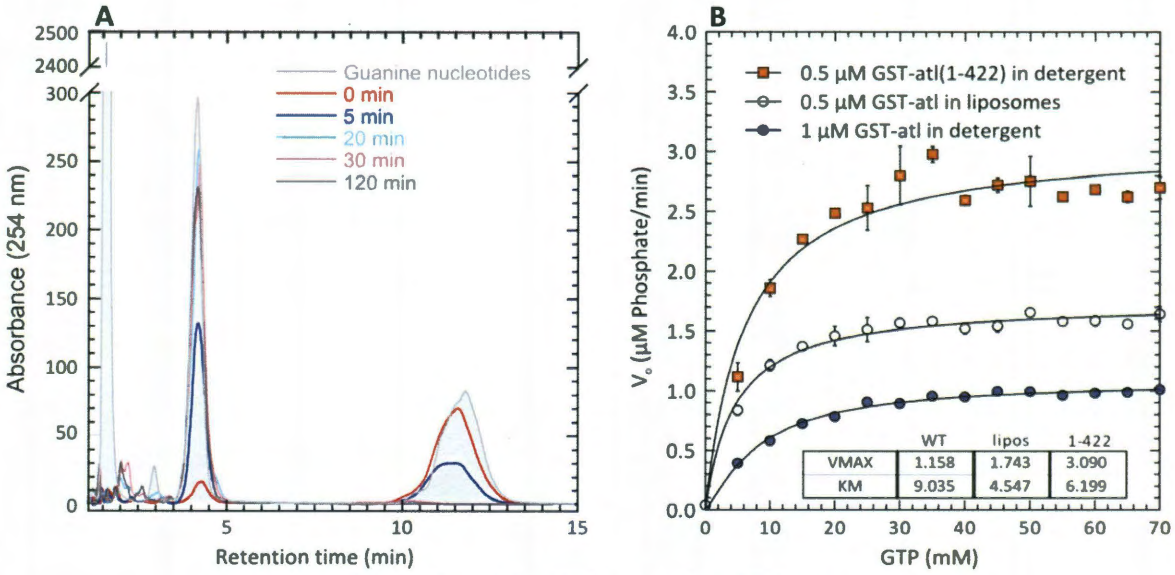


**Figure 5-1: Atlastin is an active GTPase**

(**A**)Aliquots of a GTPase reaction containing 0.5 mM GTP and 5 μM atl (1-422) from various time intervals were analyzed by HPLC. Atlastin show only GDP production. Standards of 0.5 mM GMP, GDP, and GTP were run over the column and showed peak retention times of 1.85 min, 4.4 min, and 12 min, respectively. (**B**) Michaelis-Menten kinetics of GST-atlastin in detergent compared to GST-atlastin reconstituted into liposomes and GST-atlastin (1-422). Full-length GST-atlastin shows about a 2.5 to 3-fold increase in Vmax when reconstituted into liposomes and the free cytoplasmic domain has an even greater activity (5- to 6-fold over WT in detergent). The Michaelis-Menten parameters are listed in a table inset. Error bars, SEM.

liposomes I plotted the initial velocities versus GTP concentrations and determined the $K_m$ and $K_{cat}$ of WT atlastin and atlastin$^{1-422}$ (Figure 5-1b). Surprisingly, we observed that reconstitution significantly improved the maximum velocity of this enzyme even though the amount of enzyme assayed in proteoliposomes is half (0.5 μM) of that in detergent (1μM). GTPase activity is increase while there is little difference in the binding affinities between atlastin in detergent and in liposomes. These data demonstrate that atlastin is a more active enzyme in a phospholipid bilayer compared to a detergent micelle. The most straightforward interpretation of this activity increase is that atlastin has an improved ability to dimerize in the plane of a membrane following reconstitution (a cis-dimer) or that trans dimerization between liposomes stimulates GTPase activity.

Next, I examined the activity of the N-terminal cytoplasmic domain, atl (1-422). The N-terminal cytoplasmic domain displayed stimulated activity even greater than that seen in reconstituted full length protein (Figure 5-1b and Figure 4-3)) suggesting that the regions of atlastin responsible for oligomerization and enzymatic activation reside in this domain. Given that other large GTPases like dynamin and GBP1 dimerize through contacts within the G-domain, we produced an additional construct that expressed the isolated GTPase domain, atl (1-328). However, we found that the GTPase domain alone was not sufficient to produce an active enzyme at the same concentration (0.5 μM) as the other protein examined (Figure 4-3). The atl (1-328) protein is not simply a misfolded protein because it shows a concentration dependent increase in at activity higher GTP concentrations

(Figure 4-3). These results suggest that the GTPase domain alone is not sufficient to provide a stable interaction platform for GTP hydrolysis.

## 5.2. GTP hydrolysis is required for fusion

While it is clear that atlastin is a functional GTPase it is unclear whether GTP hydrolysis or binding or both is required for atlastin-mediated membrane fusion.

Co-immunoprecipitation of HA- and Myc-tagged atlastin expressed in HeLa cells showed that atlastin-HA was co-immunoprecipitated by anti-myc antibodies (Figure 5-2a) and the addition of 1 mM GTP or GTPγS to cell lysates resulted in a 3-fold increase in complex formation between atl-myc and atl-HA (Figure 5-2a). This

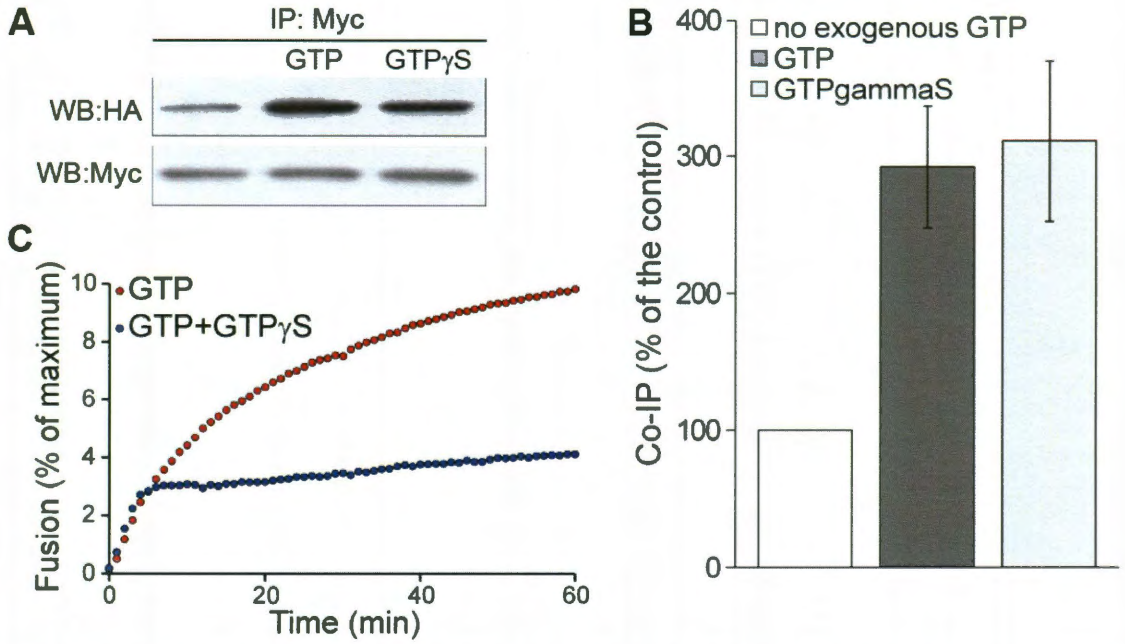


**Figure 5-2: GTPγS enhances atlastin self-association but inhibits ongoing liposome fusion.** (A) Co-immunoprecipitation of transfected atlastin-HA and atlastin-myc was performed in the absence of exogenous nucleotide or presence of 1 mM GTP or GTPγS. (B) Quantification of the data from five independent co-immunoprecipitation experiments shows that the presence of GTP and GTPγS increase atlastin complex formation. (C) Addition of 0.5 mM GTPγS to an ongoing liposome fusion reaction rapidly blocks fusion. Error bars represent S.E.M. Panels A&B by Diana Pendin

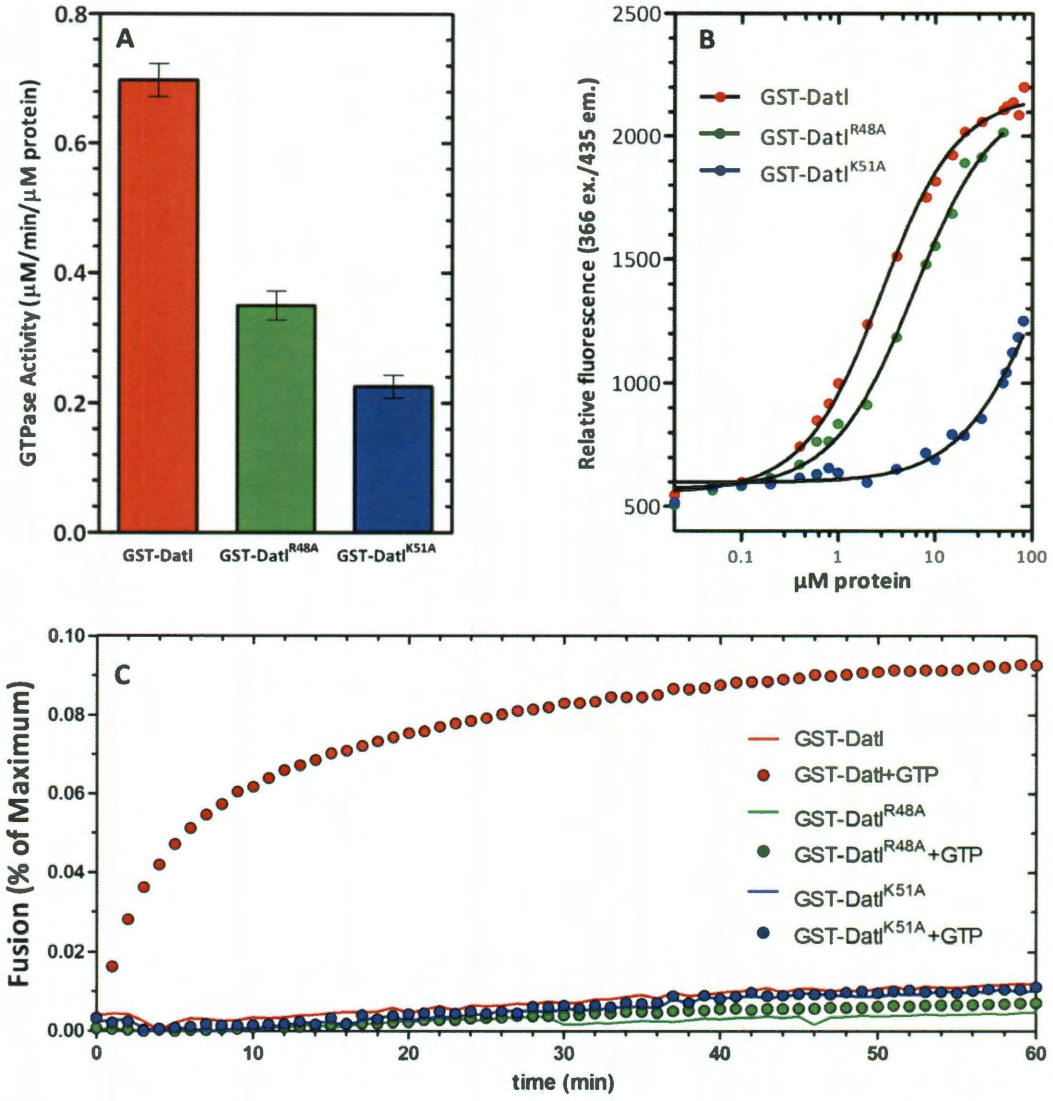


**Figure 5-3: GTP binding is not sufficient to promote membrane fusion.**
(**A**) GTPase activity of 1 μM GST-tagged protein in detergent. The active site mutations, K51A and R48E, incompletely reduce GTPase activity. Error bars, SEM. (**B**) Binding to mant-GTPγS with increasing amounts of GST-tagged atlastin mutants. The K51A mutant has a reduced binding affinity to nucleotide ($K_d$ = 134 μM ) compared to WT and the R48A mutant ($K_d$ = 2.3 μM and 5.6 μM, respectively. Data were fit with a global $F_{max}$ (see methods). (**C**) Neither of the GTPase domain mutants is able to promote membrane fusion.

is in agreement with the dimerization of atlastin (1-422) in the presence of GTPγS (Figure 4-1). Curiously while GTPγS increases atlastin association in vivo and in vitro is has been shown to inhibit in vitro ER reformation[12]. In vitro fusion results also show that GTPγS is unable to support fusion (Figure 3-3 and Figure 3-5).

Furthermore, addition of GTPγS to an ongoing fusion reaction abruptly and potently inhibits fusion (Figure 5-2). These data suggest that nucleotide binding is not enough to promote fusion. Oligomerization and possibly docking of liposomes is likely supported by GTP binding and GTP hydrolysis must ensue for fusion to occur.

Point mutations within the GTPase domain of atlastin agree with this hypothesis. A lysine to alanine mutation at residue 51 (K51A) within the active site of atlastin results in reduced GTPase activity and GTP binding (Figure 5-3 a&b) showing about a roughly 60-fold decrease in binding affinity compared to WT while an arginine to alanine mutation at reside 48 (R48A) had little effect upon binding affinity (Figure 5-3b). Even though the atlastin$^{R48A}$ mutant binds GTP similar to wildtype it is deficient in GTP hydrolysis and ineffective in promoting the fusion of liposomes supporting the idea that nucleotide binding alone is insufficient to support fusion. Atlastin must hydrolyze GTP to fuse membranes.

**Table 5-1: HSP mutations in atlastin-1 and analogous residues in *Drosphila* atlastin**

| Hs-Atl1 | Dm-Atl | Domain | Hs-Atl1 | Dm-Atl | Domain | Hs-Atl1 | Dm-Atl | Domain |
|---|---|---|---|---|---|---|---|---|
| K80A | K51 | GTPase | H247R[51] | H222 | GTPase | M408T[52] | M383 | 3-helix |
| F151S[53] | F126 | GTPase | L250P[52] | L225 | GTPase | F413L[54] | F388 | 3-helix |
| T156I[55] | T131 | GTPase | Q251K[54] | Q226 | GTPase | R415W[56] | *E390* | 3-helix |
| L157W[57] | *V132* | GTPase | V253I[54] | *L228* | GTPase | ΔN436[58] | N411 | 3-helix |
| A161P[59] | A136 | GTPase | H258R[15] | *S233* | GTPase | N440T[54] | N415 | 3-helix |
| T162P[22] | T137 | GTPase | S259F[51] | S234 | GTPase | Y459C[60] | Y434 | TMD |
| A165T[51] | A140 | GTPase | S259Y[15] | S234 | GTPase | G469A[52] | G444 | TMD |
| H189D[7] | H164 | GTPase | I315S[53] | I290 | GTPase | G482V[52] | G457 | TMD |
| Q191R[52] | Q166 | GTPase | Y336H[52] | Y311 | GTPase | A492fsX522[52] | A467 | STOP |
| R217Q[61] | R192 | GTPase | C375R[22] | C350 | 3-helix | R495W[62] | R470 | STOP |
| R239C[15] | R214 | GTPase | S398Y[53] | A373 | 3-helix | E502fsX522[63] | *D477* | STOP |
| R239L[51] | R214 | GTPase | S398F[64] | A373 | 3-helix | I507fsX522[65] | *L482* | STOP |
| H247P[59] | H222 | GTPase | M408V[66] | M383 | 3-helix | S519N[54] | *M494* | unknown |

## 5.3. Pathological mutations within the GTPase domain reduce GTPase activity and fusion activity

Unsurprisingly, the majority of the disease-causing alleles of SPG3A fall within the GTPase domain of atlastin (Table 5-1). Analogous mutation of two such alleles R239C and S259Y were made in *Drosophila* atlastin, R214C and S234Y. I measured the GTPase activity of these two alleles and found that R214C showed reduced GTPase activity (Figure 5-4). Surprisingly, although the GTPase activity was reduced to nearly the same degree as the R48A mutation, this "pathological"

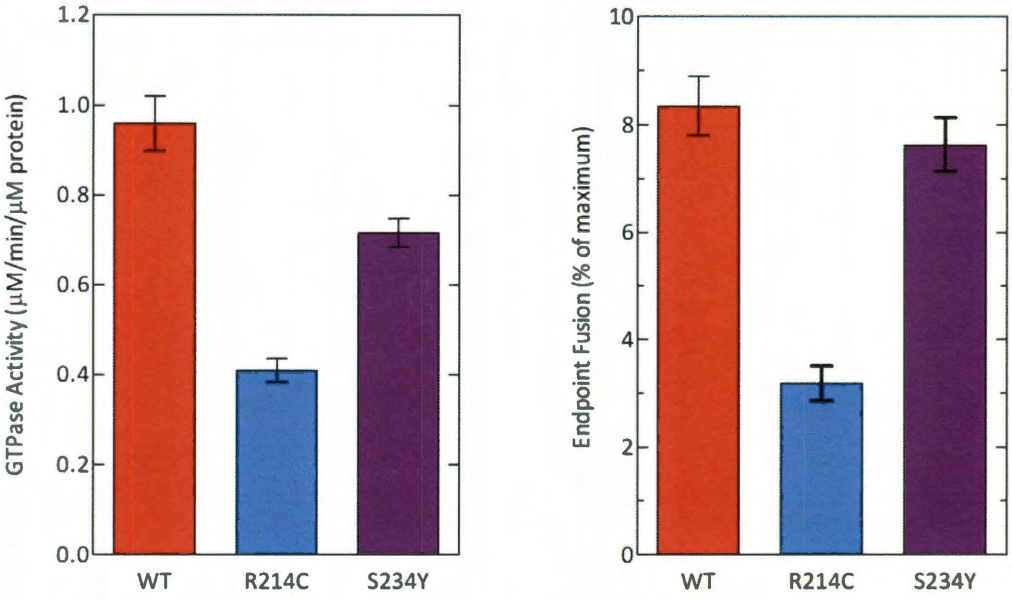


**Figure 5-4: GTPase and fusion activity of pathological mutants.**
Mutations within the GTPase domain of fly atlastin analogous to pathological mutations identified in humans show reduce GTPase activity (0.5 mM GTP, 1 μM protein). The pathological mutants are able to support some degree of fusion despite the reduced GTPase activity.

mutant was able to support fusion proportional to its level of GTPase activity. The S234Y mutation behaved similarly to wildtype in both GTPase activity and extent of fusion. This reflects that although there is strong conservation in sequence in the GTPase domain from fly atlastin to human atlastin, comparison of results between the two should be made with caution.

## 5.4. Conclusions

Data from the nonhydrolyzable nucleotides and point mutations agree that GTP binding and dimerization of atlastin are not enough to promote fusion. GTP hydrolysis and likely a conformation change are required to promote fusion. This suggests that atlastin dimerization upon nucleotide binding occurs through the GTPase domain alone and assume the shape of the form 2 dimer (Figure 4-4). However, the AUC data shows that stable dimerization requires the middle domain similar to the form 1 dimer (Figure 4-4). However, both of these experiments are done with a truncated form of atlastin where the 3HB is freer to assume either dimer form.

# Chapter 6

# The middle-domain three-helix bundle plays and important role in atlastin function

## 6.1. Proline mutations within the middle domain 3-helix bundle disrupt atlastin function

The middle domain of atlastin forms a 3-helix bundle (3HB) that provides a strong interaction surface in the form 1 crystal structure (Figure 4-4). This 3HB is important in forming or stabilizing a dimer in the *Drosophila* atlastin N-terminal cytoplasmic domain (Figure 4-1). Additionally, GTPase activity is impaired in a soluble domain lacking the 3HB, atlastin (1-328). The importance of the 3HB in the context of full-length atlastin was done by introducing proline-mutations that would disrupt the α-helical nature of this domain. I purified and reconstituted full-length atlastin with proline mutations at residues leucine 400 and phenylalanine 404,

L400P and F404P respectively. I tested the affect these mutations have upon GTPase activity and the ability to promote fusion.

When tested for fusion both proline mutations were unable to promote fusion (Figure6-1). The GTPase activity of atlastin is increased when atlastin is reconstituted into a lipid bilayer (Figure 5-1). This may be due to the cooperative nature of large GTPases. The self-association of atlastin monomers would likely be increased when restricted to the plane of the lipid bilayer resulting in increased

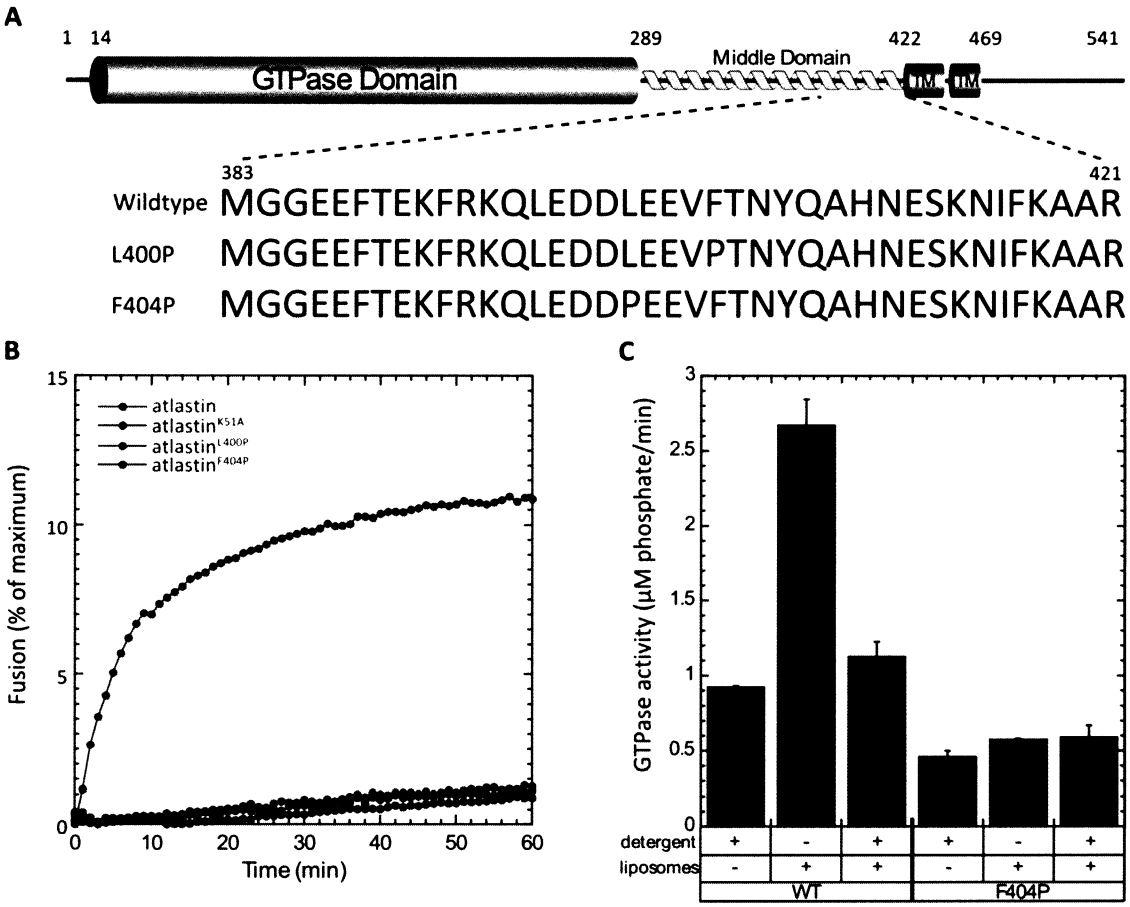


**Figure 6-1: Proline mutations in the 3-helix bundle disrupt atlastin function**
(A) Cartoon schematic showing the location of the proline mutations in the 3HB domain. (B) The 3HB proline mutants cannot fuse liposomes. (**C**) The reconstitution induced stimulation in GTPase activity is dependent upon the 3HB domain. Wildtype atlastin shows a 2.5-3 fold increase in GTPase activity when in liposomes while the F404P atlastin mutant does not show any increase in activity. Errors bars, SEM.

GTPase activity. This hypothesis would predict that if homooligomerization were disrupted there would be no increase in GTPase activity upon reconstitution. There is no increase in GTPase activity when the atlastin$^{F404P}$ mutant is reconstituted into liposomes (Figure 6-1)

## 6.2. The full-length soluble domain of atlastin is a potent inhibitor of atlastin mediated membrane fusion

All membrane fusion proteins characterized to date require membrane integration. However, liberated soluble domains that retain the ability to productively interact with membrane integral components are often inhibitors of fusion. This is definitely the case for SNARE proteins and inclusion of a soluble fragment of either v-SNARE or t-SNARE component will inhibit fusion[37,67]. I tested the functionality of C-terminal truncations that lack a membrane spanning domain by determining their capacity to inhibit fusion between proteoliposomes that contain wildtype atlastin. I tested atlastin (1-422) that encompassed the entire N-terminal cytoplasmic domain and atlastin (1-328) that contains the isolated GTPase domain. When atlastin (1-422) was titrated into a fusion reaction containing wildtype atlastin in the membrane, progressive inhibition of both the rate and extent of membrane fusion is seen (Figure 6-2). Inhibition was concentration dependent and fusion was completely inhibited with a 6-fold molar excess of the atlastin (1-422) soluble domain. While the full-length N-terminal cytoplasmic

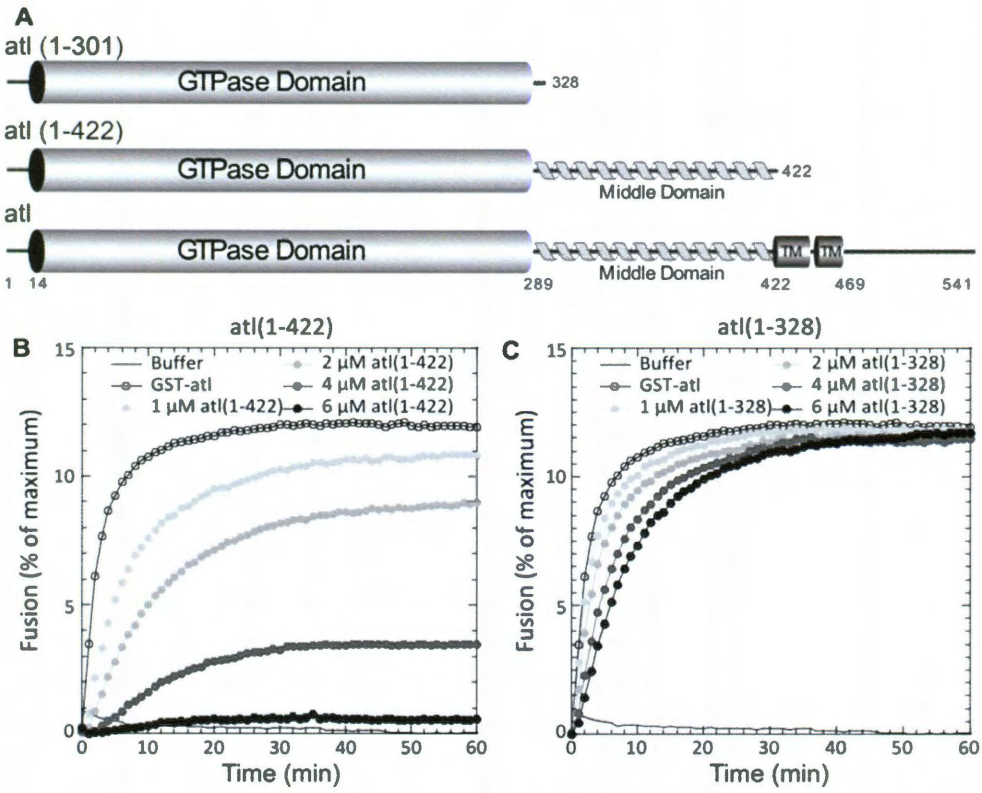


**Figure 6-2: Atlastin soluble domain inhibiton of atlastin mediated fusion** (**A**) Cartoon schematic of atlastin fragments purified and added acutely to fusion reactions between GST-atlastin proteoliposomes (**B** and **C**). (**B**) Atlastin (1-422) inhibits fusion in a dose dependent manner and completely inhibits fusion at a 6 molar excess of protein. (**C**) Atlastin (1-328) shows minimal inhibition of fusion over the same range of concentrations.

domain was a potent inhibitor, the isolated GTPase domain (atl (1-328)) was ineffective in inhibited fusion.

## 6.3. The proximity of the 3HB to the transmembrane domains is important for fusion activity

Association of the 3HB is important for the fusogenicity of atlastin. The association of the two 3HBs in the form 1 crystal structure (Figure 4-4) would

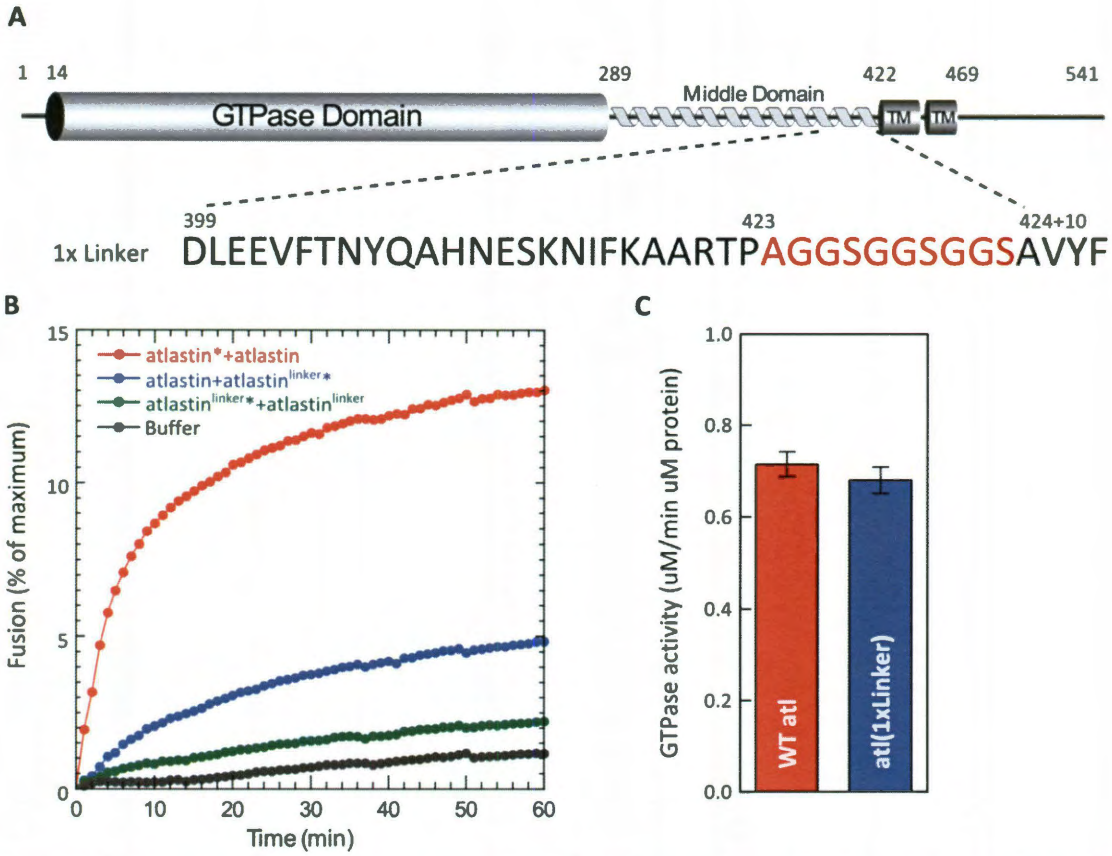


**Figure 6-3: Insertion of a juxtamembrane flexible linker reduces the fusogenicity of atlastin**
(**A**) Schematic representation of the location of the insertion of a flexible linker between the 3HB and the transmembrane domains. (**B**) Fusion is decreased when wildtype unlabeled liposomes are fused with linker mutant liposomes (asterisk denotes labeled liposomes). Fusion is further decreased when both populations of liposomes contain the mutant protein. (**C**) The atlastin linker mutant has similar GTPase activity to wildtype. Error bars, SEM.

require very close apposition of distinct bilayers in a trans-dimer forcing fusion to occur so that the two subunits reside in the same bilayer (cis-dimer). To test the importance of the proximity of the base of the 3HB to the membrane a flexible 3X Gly-Gly-Ser-linker was inserted in the juxtamembrane region between proline -423 and alanine-424 (Atlastin(1xlinker), Figure 6-3) to distance the 3HB from the membrane. A similar mutation was made in the SNAREs syntaxin1a and Vamp2. These flexible linkers reduce the ability of SNARES to promote fusion[68], by uncoupling the energy release by formation of the ternary SNARE complex from

being transduced through the transmembrane domain into the lipid bilayer. The atlastin (1xlinker) has reduced ability to fuse liposomes (Figure 6-3).

## 6.4. Conclusions

The middle domain 3HB of atlastin is important in mediating stable self-association of atlastin. Disruption of the 3HB results in a reduction in GTPase activity and a loss of fusogenic ability (Figure 6-1). Soluble domain inhibition studies show that the GTPase domain alone lacking the 3HB is insufficient to mediate tight association. However the full-length N- terminal cytoplasmic domain including the 3HB binds tightly and is a potent inhibitor of atlastin proteoliposomes fusion (Figure 6-2). The proximity of the 3HB to the membrane is important. Formation of trans-dimers that tightly associate through the 3HB are important in efficient membrane fusion as when the 3HB is distanced from the membrane via a flexible linker fusion is impaired (Figure 6-3).

# Chapter 7

# The C-terminal cytoplasmic domain

## 7.1. The C-terminal cytoplasmic domain of atlastin is required for fusion

To explore the requirement of other domains of atlastin we made several large truncations at the C-terminus. We started making deletions from the C-terminal end as we have shown that GTPase activity is required for fusion and the GTPase domain is found near the N-terminus. We produced truncations that removed the entire C-terminal cytoplasmic domain (residues 472-542) and the second transmembrane domain as well as the C-terminal cytoplasmic domain (residues 451-542). Both resulting atlastin fragments, atlastin (1-450) and atlastin (1-471), retain an intact GTPase domain and at least one transmembrane anchor(Figure 7-1a). We expressed these proteins in E. coli and reconstituted them into synthetic PCPS liposomes and measured membrane fusion by lipid mixing.

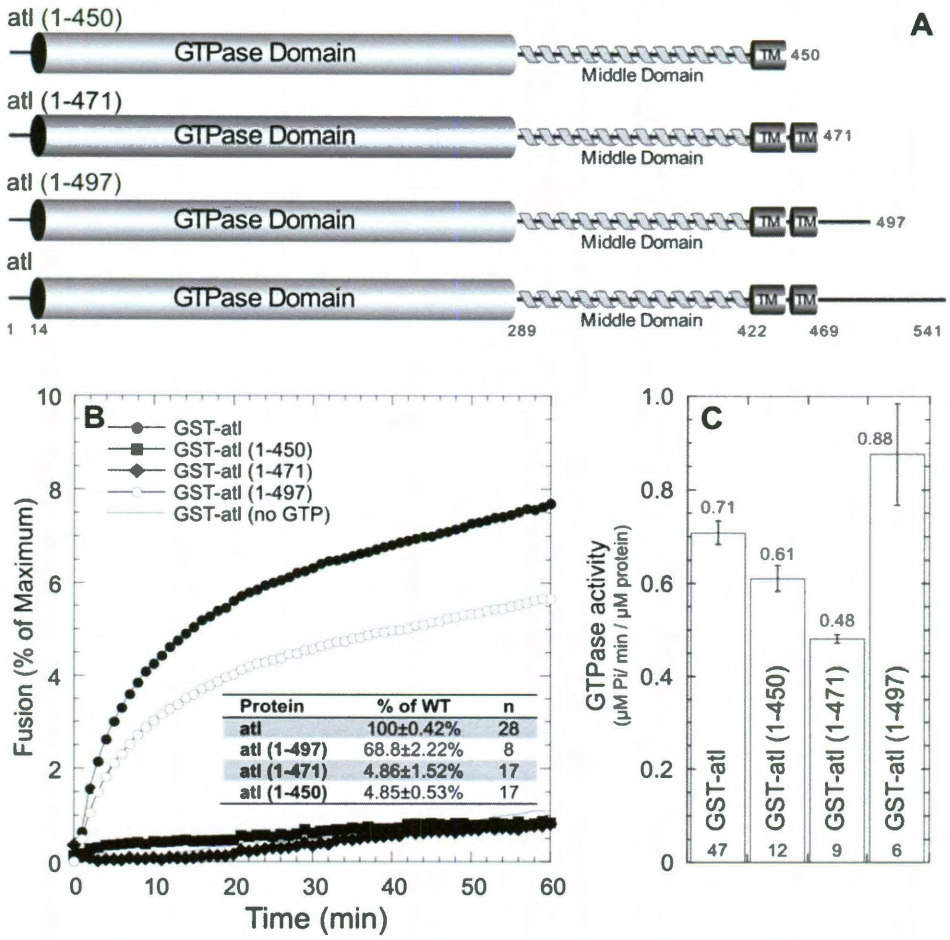


**Figure 7-1: C-terminal truncations of atlastin are unable to fuse liposomes**
(A) Domain structure of atlastin and the c-terminal truncations. **(B)** Kinetic fusion graph of unlabeled atlastin acceptor proteoliposomes fused with equimolar amounts of fluorescently labeled atlastin donor proteoliposomes **(Inset)** The average extent of fusion at 60 min is represented in a table as percent of WT fusion for all mutants. **(C)** GTPase activity of all the mutants. Error bars, SEM.

When either of these two proteins was reconstituted into proteoliposomes, no fusion was observed (Figure 7-1b). The functionality of these enzymes was confirmed by examining GTPase activity (Figure 7-1c). Both 1-450 and 1-471 were able of cleaving GTP at rates that were within 25% of wildtype. These results suggest that the C-terminal cytoplasmic domain of atlastin is critical for membrane fusion.

The C-terminal truncation, atlastin (1-471), was also assayed for its fusogenic ability in vivo. Cos7 cells overexpressing wildtype atlastin have an abnormal punctate ER (Figure 7-2a,b&c). When overexpressing atlastin (1-471) the cells have a normal ER phenotype suggesting it is a non-functional protein (Figure 7-2d,e&f).

The C-terminal domain of atlastin is among the most divergent between

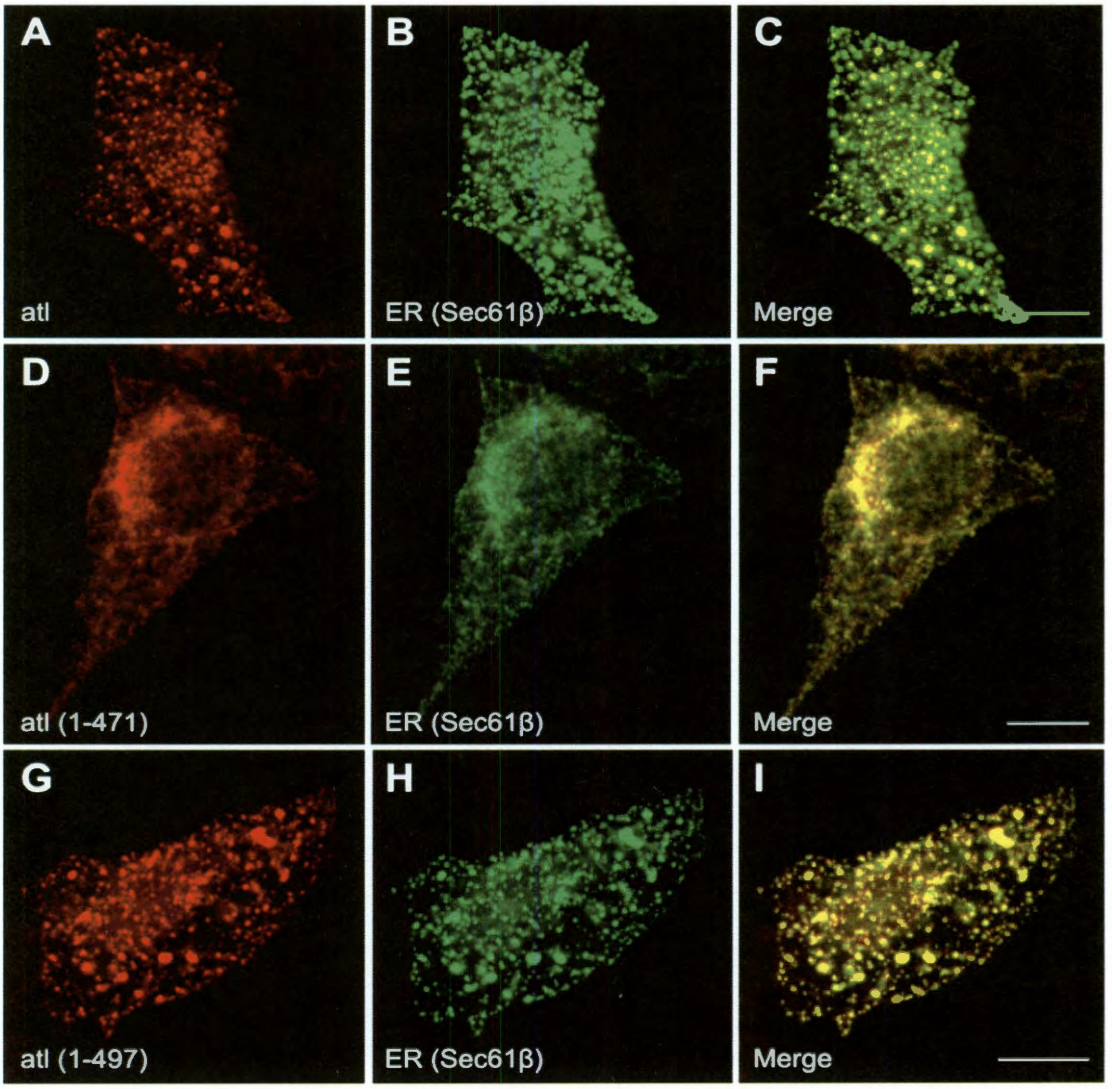


**Figure 7-2: Deletion of c-terminal domain results in a non-functional protein in vivo.** Cos7 cells were cotransfected with wildtype atl-myc (**A-C**), atl (1-471)-myc (**D-F**), or atl (1-497)-myc (**G-I**) and GFP-Sec61β. Wildtype atl and atl (1-497) show an abnormal, punctate ER indicating a functional Drosophila atlastin protein, while atl (1-471) localizes to a normally reticular ER suggesting that it is a nonfunctional protein. Scale bar, 10 μm. Data by D. Pendin

atlastin homologs and paralogs. Closer inspection of the sequences that comprise the C-terminal cytoplasmic domain revealed an approximately 25 amino acid stretch of more highly conserved residues membrane proximal to the second transmembrane domain followed by a very divergent extreme C-terminus. We further subdivided the C-terminal cytoplasmic domain to add back the more conserved juxtamembrane region (residues 471-497). The resulting construct (1-497) was also expressed, reconstituted and assayed for membrane fusion. Figure 7-1 demonstrates that the reintroduction of these 27 residues restores approximately 75% of wildtype fusion activity and Cos7 cells overexpressing atlastin (1-479) have a punctate ER (Figure 7-2g,h&i) similar to wildtype atlastin overexpression.

## 7.2. Conclusions

In vitro (Figure 7-1) and in vivo (Figure 7-2) data suggest a short region of approximately 27 amino acids located within the cytoplasmic C-terminal domain are critically required for atlastin-dependent membrane fusion. Interestingly, three frame shift mutations in human Atlastin-1, A492fsX522, E502fsX522, and I507fsX522 (Table 5-1), known to cause hereditary spastic paraplegia, prematurely truncate Atlastin-1 and scramble the C-terminal juxtamembrane region that we have shown is required for membrane fusion.

While the function of this region is unclear, the C-terminal region appears to show a propensity to form amphipathic helices (Figure 7-3). Additionally, preliminary data show that introduction of charged residues in the hydrophobic face of a putative amphipathic α-helix disrupts fusion (Figure 7-4a). Also, swapping

out the entire C-terminal region of fly atlastin with an analogous region from human atlastin-1 or -3 results in a fusogenic chimaera. This suggests that this region does not have a specific interaction and probably has a propensity to interact with the adjacent lipid bilayer,

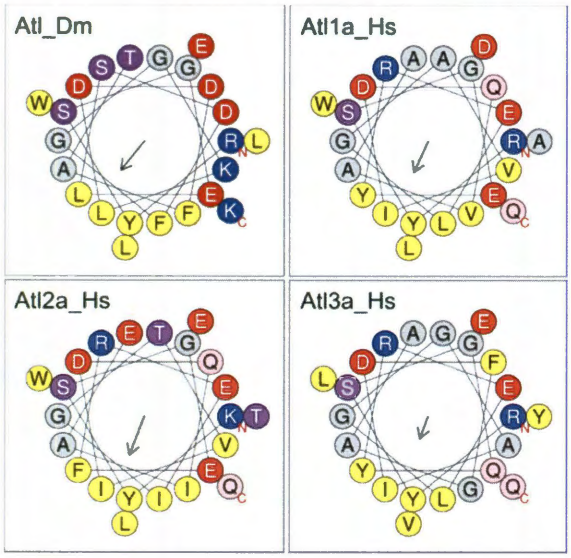


**Figure 7-3: Helical wheel projections of the juxta-membrane c-terminal region on atlastin**
The 23-residue juxtamembrane regions of fly atlastin and the three human isoforms of atlastin were analyzed for their propensity to from amphipathic helices by the program HeliQuest (http://heliquest.ipmc.cnrs.fr/).

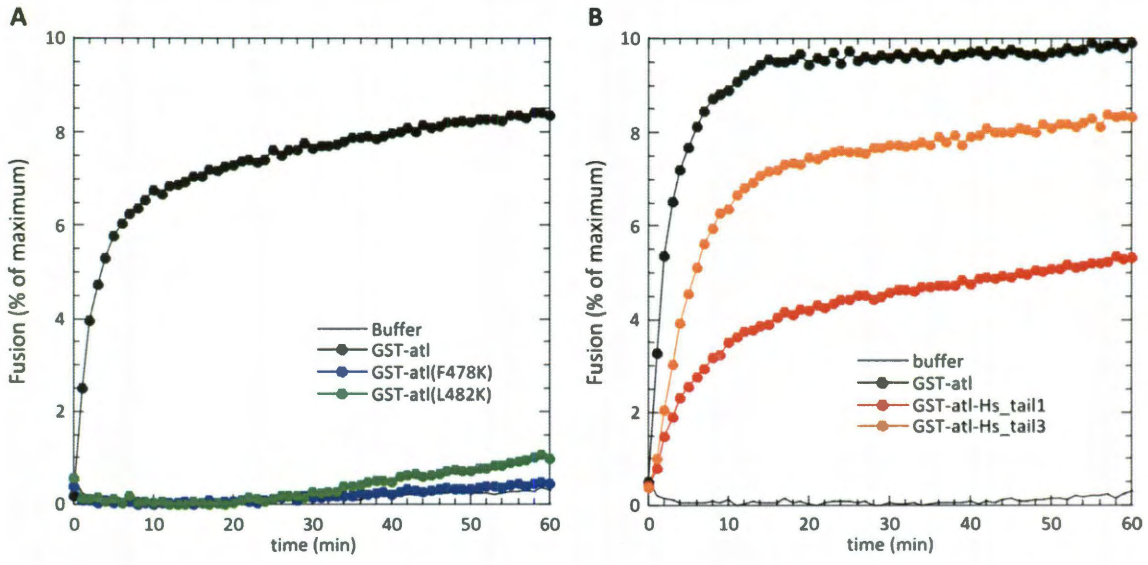


**Figure 7-4: Preliminary data of c-tail mutants and human c-terminal domain swaps.**
(A) Kinetic fusion graph of GST-atlastin, GST-atlastin (F478K), or GST-atlastin (L482K). Charge mutations at targeted positions within the c-terminal domain abolish atlastin fusogenicity. (B) Kinetic fusion graph of liposomes bearing wildtype atlastin or atlastin mutants that swapped out the the c-terminal domain of atlastin for the respective sequence of human atlastin 1 and atlastin 3 isoforms.

# Chapter 8

# Discussion

## 8.1. Model of atlastin mediated fusion

Membrane fusion by atlastin likely involves many steps. The schematic shown in Figure 8-1 describes our working model for atlastin function. Atlastin almost entirely faces the cytoplasm with as few as 5 residues in an ER luminal loop. We suggest that the fusion cycle begins with nucleotide-free atlastin monomers (Figure 8-1a ) in opposing ER membranes. These monomer forms are cartooned as the "pre-fusion" (31) or crystal form 2 structures (34). Then we suggest that nucleotide binding (Figure 8-1b) results in a permissive state for association between the GTPase domains (Figure 8-1c ). The N-terminal cytoplasmic domain of Drosophila atlastin (Atl (1-422)) forms a dimer when bound to nonhydrolyzable GTPγS but not with GDP (Figure 4-1). We assume that this association also occurs in the context of full length atlastin. While this interaction between the GTPase

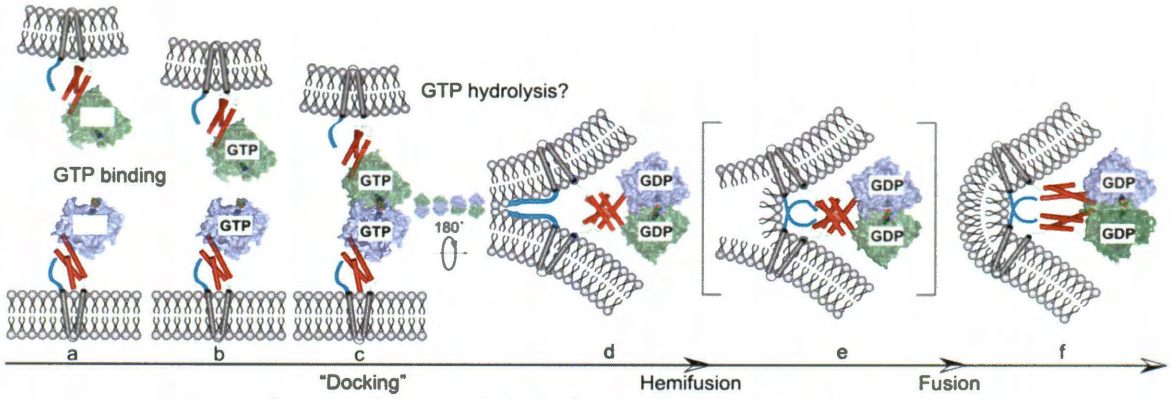


**Figure 8-1: Working model of atlastin mediated membrane fusion**

domains is presumably a required intermediate, its stability may be limited. We propose that the interaction between GTPase domains matures to a more stable dimer facilitated primarily by an interaction between the middle domain three helical bundle segments (Figure 8-1d). This conformational change is achieved, perhaps driven by nucleotide hydrolysis, by rotating the GTPase domain dimer 180 degrees which forces the three-helix bundles into close proximity. The new association between adjacent 3HBs liberates the C-terminal tail domain to perform its required role. We have localized this required function to a region of 27 amino acids immediately adjacent to the second transmembrane span (Figure 7-1). The activity of this C-terminal domain may be accomplished by forming a new association with the dimeric 3HB or by direct interaction with lipid (Figure 8-1d). We currently favor a direct interaction with lipid based on the amphipathic nature of this protein sequence (Figure 7-3). An interaction between the membrane surface and the amphipathic C-terminal tail could destabilize the bilayer and provide the driving force for outer leaflet mixing, resulting in a hemifusion intermediate (Figure 8-1e) that resolves by inner leaflet mixing to full fusion (Figure

8-1f). The resulting cis-dimer resembles the "post fusion"[48] or crystal form 1 structure[46]. Finally, we hypothesize that GDP release could then promote dissociation.

Although, the precise location and timing of GTP hydrolysis during the cycle is speculative, some biochemical experiments can be used to place constraints on the model. We suggest that the large conformational change postulated to occur following docking (Figure 8-1c&d) utilizes the energy provided by GTP hydrolysis. However our oligomerization data suggest that GTPγS, but not GDP, results in the stable dimeric conformation cartooned in Figure 8-1d when soluble fragments are examined, indicating that this intermediate may contain bound GTP. Functional analysis revealed that GTP hydrolysis is required to fuse proteoliposomes in vitro since GTPγS does not support fusion[40]. These lipid mixing results demonstrate that nucleotide hydrolysis is required prior to hemifusion; however, we cannot exclude the possibility that events downstream of GTP hydrolysis, for example inorganic phosphate release, play an important role[48].

# References


1. Martens, S. & McMahon, H.T. Mechanisms of membrane fusion: disparate players and common principles. *Nature Reviews Molecular Cell Biology* **9**, 543–556 (2008).

2. Ungermann, C. & Langosch, D. Functions of SNAREs in intracellular membrane fusion and lipid bilayer mixing. *J Cell Sci* **118**, 3819-3828 (2005).

3. Blumenthal, R., Clague, M.J., Durell, S.R. & Epands, R.M. Membrane fusion. *Chem. Rev* **103**, 53–70 (2003).

4. Chen, Y.A. & Scheller, R.H. SNARE-mediated membrane fusion. *Nat. Rev. Mol. Cell Biol* **2**, 98–106 (2001).

5. Evans, K. *et al.* Interaction of two hereditary spastic paraplegia gene products, spastin and atlastin, suggests a common pathway for axonal maintenance. *Proc. Natl. Acad. Sci. U.S.A* **103**, 10666-10671 (2006).

6. Park, S.H., Zhu, P.-P., Parker, R.L. & Blackstone, C. Hereditary spastic paraplegia proteins REEP1, spastin, and atlastin-1 coordinate microtubule interactions with the tubular ER network. *J. Clin. Invest* **120**, 1097-1110 (2010).

7. Lee, Y. *et al.* Loss of spastic paraplegia gene atlastin induces age-dependent death of dopaminergic neurons in Drosophila. *Neurobiol. Aging* **29**, 84-94 (2008).

8. Voeltz, G.K., Rolls, M.M. & Rapoport, T.A. Structural organization of the endoplasmic reticulum. *EMBO reports* **3**, 944 (2002).

9. Vedrenne, C. & Hauri, H.P. Morphogenesis of the endoplasmic reticulum: beyond active membrane expansion. *Traffic* **7**, 639–646 (2006).

10. Kano, F. *et al.* NSF/SNAPs and p97/p47/VCIP135 are sequentially required for cell cycle-dependent reformation of the ER network. *Genes Cells* **10**, 989-999 (2005).

11. Nakajima, K. *et al.* Involvement of BNIP1 in apoptosis and endoplasmic reticulum membrane fusion. *The EMBO Journal* **23**, 3216 (2004).

12. Dreier, L. & Rapoport, T.A. In vitro formation of the endoplasmic reticulum occurs independently of microtubules by a controlled fusion reaction. *Journal of Cell Biology* **148**, 883 (2000).

13. Orso, G. *et al.* Homotypic fusion of ER membranes requires the dynamin-like GTPase Atlastin. *Nature* **460**, 978-983 (2009).

14. Hu, J. *et al.* A class of dynamin-like GTPases involved in the generation of the tubular ER network. *Cell* **138**, 549-561 (2009).

15. Zhao, X. *et al.* Mutations in a newly identified GTPase gene cause autosomal dominant hereditary spastic paraplegia. *Nat. Genet.* **29**, 326-331 (2001).

16. Fink, J.K. Advances in the hereditary spastic paraplegias. *Exp. Neurol.* **184 Suppl 1**, S106-110 (2003).

17. Salinas, S., Proukakis, C., Crosby, A. & Warner, T.T. Hereditary spastic paraplegia: clinical features and pathogenetic mechanisms. *Lancet Neurol* **7**, 1127-1138 (2008).

18. Dürr, A. Genetic testing for the spastic paraplegias: drowning by numbers. *Neurology* **71**, 236-238 (2008).

19. Espinós, C. & Palau, F. Genetics and pathogenesis of inherited ataxias and spastic paraplegias. *Adv. Exp. Med. Biol.* **652**, 263-296 (2009).

20. Soderblom, C. & Blackstone, C. Traffic accidents: molecular genetic insights into the pathogenesis of the hereditary spastic paraplegias. *Pharmacol. Ther.* **109**, 42-56 (2006).

21. Hazan, J. *et al.* Spastin, a new AAA protein, is altered in the most frequent form of autosomal dominant spastic paraplegia. *Nat. Genet.* **23**, 296-303 (1999).

22. Namekawa, M. *et al.* SPG3A is the most frequent cause of hereditary spastic paraplegia with onset before age 10 years. *Neurology* **66**, 112-114 (2006).

23. Zhu, P.-P. *et al.* Cellular localization, oligomerization, and membrane association of the hereditary spastic paraplegia 3A (SPG3A) protein atlastin. *J. Biol. Chem* **278**, 49063-49071 (2003).

24. Sanderson, C.M. *et al.* Spastin and atlastin, two proteins mutated in autosomal-dominant hereditary spastic paraplegia, are binding partners. *Hum. Mol. Genet* **15**, 307-318 (2006).

25. Namekawa, M. *et al.* Mutations in the SPG3A gene encoding the GTPase atlastin interfere with vesicle trafficking in the ER/Golgi interface and Golgi morphogenesis. *Mol. Cell. Neurosci* **35**, 1-13 (2007).

26. Rismanchi, N., Soderblom, C., Stadler, J., Zhu, P.-P. & Blackstone, C. Atlastin GTPases are required for Golgi apparatus and ER morphogenesis. *Hum. Mol. Genet* **17**, 1591-1604 (2008).

27. Chen, J., Stefano, G., Brandizzi, F. & Zheng, H. Arabidopsis RHD3 mediates the generation of the tubular ER network and is required for Golgi distribution and motility in plant cells. *J. Cell. Sci.* **124**, 2241-2252 (2011).

28. Albin, R.L., Koeppe, R.A., Rainier, S. & Fink, J.K. Normal dopaminergic nigrostriatal innervation in SPG3A hereditary spastic paraplegia. *J. Neurogenet* **22**, 289-294 (2008).

29. Lee, M. *et al.* Drosophila Atlastin regulates the stability of muscle microtubules and is required for synapse development. *Dev. Biol* **330**, 250-262 (2009).

30. Malakhov, M.P. *et al.* SUMO fusions and SUMO-specific protease for efficient expression and purification of proteins. *Journal of structural and functional genomics* **5**, 75–86 (2004).

31. Ho, S.N., Hunt, H.D., Horton, R.M., Pullen, J.K. & Pease, L.R. Site-directed mutagenesis by overlap extension using the polymerase chain reaction. *Gene* **77**, 51–59 (1989).

32. Bertani, G. Studies on lysogenesis. I. The mode of phage liberation by lysogenic Escherichia coli. *J. Bacteriol.* **62**, 293-300 (1951).

33. Schaffner, W. & Weissmann, C. A rapid, sensitive, and specific method for the determination of protein in dilute solution. *Anal. Biochem* **56**, 502-514 (1973).

34. Bradford, M.M. A rapid and sensitive method for the quantitation of microgram quantities of protein utilizing the principle of protein-dye binding. *Analytical biochemistry* **72**, 248–254 (1976).

35. Schaub, J.R., Lu, X., Doneske, B., Shin, Y.-K. & McNew, J.A. Hemifusion arrest by complexin is relieved by Ca2+–synaptotagmin I. *Nat Struct Mol Biol* **13**, 748-750 (2006).

36. Rigaud, J.L., Pitard, B. & Levy, D. Reconstitution of membrane proteins into liposomes: application to energy-transducing membrane proteins. *Bba-Bioenergetics* **1231**, 223–246 (1995).

37. Weber, T. *et al.* SNAREpins: minimal machinery for membrane fusion. *Cell* **92**, 759–772 (1998).

38. Kunzelmann, S., Praefcke, G.J. & Herrmann, C. Nucleotide binding and self-stimulated GTPase activity of human guanylate-binding protein 1 (hGBP1). *Methods in enzymology* **404**, 512 (2005).

39. Demeler, B. *UltraScan: a comprehensive data analysis software package for analytical ultracentrifugation experiments.* (current version).at <http://www.ultrascan.uthscsa.edu>

40. Orso, G. *et al.* Homotypic fusion of ER membranes requires the dynamin-like GTPase Atlastin. *Nature* **460**, 978-983 (2009).

41. Brand, A.H. & Perrimon, N. Targeted gene expression as a means of altering cell fates and generating dominant phenotypes. *Development* **118**, 401-415 (1993).

42. Snapp, E.L., Iida, T., Frescas, D., Lippincott-Schwartz, J. & Lilly, M.A. The fusome mediates intercellular endoplasmic reticulum connectivity in Drosophila ovarian cysts. *Mol. Biol. Cell* **15**, 4512-4521 (2004).

43. Lippincott-Schwartz, J., Snapp, E. & Kenworthy, A. Studying protein dynamics in living cells. *Nat. Rev. Mol. Cell Biol.* **2**, 444-456 (2001).

44. Rigaud, J.L. & others Reconstitution of membrane proteins into liposomes. *Methods in enzymology* **372**, 65–86 (2003).

45. Sweitzer, S.M. & Hinshaw, J.E. Dynamin undergoes a GTP-dependent conformational change causing vesiculation. *Cell* **93**, 1021–1030 (1998).

46. Byrnes, L.J. & Sondermann, H. Structural basis for the nucleotide-dependent dimerization of the large G protein atlastin-1/SPG3A. *Proceedings of the National Academy of Sciences* **108**, 2216 (2011).

47. Moss, T.J., Andreazza, C., Verma, A., Daga, A. & McNew, J.A. Membrane fusion by the GTPase atlastin requires a conserved C-terminal cytoplasmic tail and dimerization through the middle domain. *Proceedings of the National Academy of Sciences* **108**, 11133 -11138 (2011).

48. Bian, X. *et al.* Structures of the atlastin GTPase provide insight into homotypic fusion of endoplasmic reticulum membranes. *Proceedings of the National Academy of Sciences* (2011).

49. Ghosh, A., Praefcke, G.J.K., Renault, L., Wittinghofer, A. & Herrmann, C. How guanylate-binding proteins achieve assembly-stimulated processive cleavage of GTP to GMP. *Nature* **440**, 101-104 (2006).

50. Praefcke, G.J.. & McMahon, H.T. The dynamin superfamily: universal membrane tubulation and fission molecules? *Nature Reviews Molecular Cell Biology* **5**, 133–147 (2004).

51. Smith, B.N. *et al.* Four novel SPG3A/atlastin mutations identified in autosomal dominant hereditary spastic paraplegia kindreds with intra-familial variability in age of onset and complex phenotype. *Clin. Genet* **75**, 485-489 (2009).

52. Ivanova, N. *et al.* Hereditary spastic paraplegia 3A associated with axonal neuropathy. *Arch. Neurol.* **64**, 706-713 (2007).

53. Abel, A. *et al.* Early onset autosomal dominant spastic paraplegia caused by novel mutations in SPG3A. *Neurogenetics* **5**, 239-243 (2004).

54. Dürr, A. *et al.* Atlastin1 mutations are frequent in young-onset autosomal dominant spastic paraplegia. *Arch. Neurol.* **61**, 1867-1872 (2004).

55. Hedera, P., Fenichel, G.M., Blair, M. & Haines, J.L. Novel mutation in the SPG3A gene in an African American family with an early onset of hereditary spastic paraplegia. *Arch. Neurol.* **61**, 1600-1603 (2004).

56. D'Amico, A. *et al.* Incomplete penetrance in an SPG3A-linked family with a new mutation in the atlastin gene. *Neurology* **62**, 2138-2139 (2004).

57. Rainier, S., Sher, C., Reish, O., Thomas, D. & Fink, J.K. De novo occurrence of novel SPG3A/atlastin mutation presenting as cerebral palsy. *Arch. Neurol* **63**, 445-447 (2006).

58. Meijer, I.A. *et al.* Characterization of a novel SPG3A deletion in a French-Canadian family. *Ann. Neurol* **61**, 599-603 (2007).

59. Sauter, S.M., Engel, W., Neumann, L.M., Kunze, J. & Neesen, J. Novel mutations in the Atlastin gene (SPG3A) in families with autosomal dominant hereditary spastic paraplegia and evidence for late onset forms of HSP linked to the SPG3A locus. *Hum. Mutat* **23**, 98 (2004).

60. Matsui, M. *et al.* A novel mutation in the SPG3A gene (atlastin) in hereditary spastic paraplegia. *J. Neurol* **254**, 972-974 (2007).

61. Muglia, M. *et al.* Further evidence that SPG3A gene mutations cause autosomal dominant hereditary spastic paraplegia. *Ann. Neurol.* **51**, 794-795 (2002).

62. Scarano, V. *et al.* The R495W mutation in SPG3A causes spastic paraplegia associated with axonal neuropathy. *J. Neurol* **252**, 901-903 (2005).

63. Loureiro, J.L. *et al.* Novel SPG3A and SPG4 mutations in dominant spastic paraplegia families. *Acta Neurologica Scandinavica* **119**, 113-118 (2009).

64. Fusco, C. *et al.* Hereditary spastic paraplegia and axonal motor neuropathy caused by a novel SPG3A de novo mutation. *Brain Dev* (2009).doi:10.1016/j.braindev.2009.08.003

65. Tessa, A. *et al.* SPG3A: An additional family carrying a new atlastin mutation. *Neurology* **59**, 2002-2005 (2002).

66. Dalpozzo, F. *et al.* Infancy onset hereditary spastic paraplegia associated with a novel atlastin mutation. *Neurology* **61**, 580-581 (2003).

67. McNew, J.A. *et al.* Compartmental specificity of cellular membrane fusion encoded in SNARE proteins. *Nature* **407**, 153-159 (2000).

68. McNew, J.A., Weber, T., Engelman, D.M., Söllner, T.H. & Rothman, J.E. The Length of the Flexible SNAREpin Juxtamembrane Region Is a Critical Determinant of SNARE-Dependent Fusion. *Molecular Cell* **4**, 415-421 (1999).